AIAA JOURNAL
Vol. 43, No. 12, December 2005

Free Vibrations of Bonded Single Lap Joints in Composite, Shallow Cylindrical Shell Panels

Umur Yuceoglu* and Varlık Özerciyes†
Middle East Technical University, 06531 Ankara, Turkey

The problem of free vibrations of bonded single lap joints in composite, shallow circular cylindrical shells or shell panels is investigated. The shallow circular cylindrical shell adherends are considered to be made of dissimilar, orthotropic materials adhesively bonded by an in-between, very thin, yet flexible adhesive layer. In the theoretical formulation, a first-order shear deformation shell theory is employed. The complete set of shallow shell equations, in combination with the adhesive-layer equations, is first reduced to a governing system of first-order ordinary differential equations in the state vector form. Then, the resulting equations are integrated by the modified transfer matrix method (with interpolation polynomials and/or Chebyshev polynomials) and the natural frequencies and the modes of the lap joint system are obtained. It was found that the hard and the soft adhesive-layer elastic constants significantly influence the natural frequencies of the shallow shell bonded lap joint system. Also, the effects of some other important parameters on the natural frequencies and the mode shapes are presented.

Introduction

AIR and space vehicle structures, such as aircraft, spacecraft, booster, and rocket structures, are mainly composed of plate and shell elements. So-called advanced composites in the form of multilayer stiffened and/or unstiffened plate and full or shallow shells increasingly are being used in these structural systems. The current trend clearly shows that a high percentage of fighter and business aircraft structures are manufactured using advanced composites.[1–3]

Advanced metal alloy and/or advanced composite systems in aerospace structures are mostly in the form of shallow shells and/or curved plates or panels. Furthermore, the joining and the extension of the multi- or single-layer, composite aerostructures are constructed in the form of adhesively bonded single lap joints.[1,3]

At this point, a few words on the motivation for this study are in order. The available scientific and engineering literature on full and shallow shells is exhaustive. However, to the best knowledge of the present authors, investigations on elastostatics and elastodynamics of single lap joints in isotropic or composite shells are few. Those studies available in the literature concentrate on tubular lap joints and not shell lap joints. Also, in their analytical formulations, relatively simple theories[4–6] based on the mechanics of materials approach are employed rather than shell theories.

The elastostatic stress concentrations in bonded single lap joints in composite, full circular cylindrical shells were first investigated by Yuceoglu and Updike.[7–9] They used a first-order shear deformation shell theory (FSDST). Research studies on the dynamics and vibrations of lap joints in shell-type structures, however, are few if not nonexistent.

Therefore, this study aims to analyze and to investigate the free vibrations of bonded single lap joints in composite, shallow circular cylindrical shells or shell panels. The present work is, mainly, an extension of some recent research work by the present authors[10–15] on the dynamics and vibrations of composite plate and shell panels and their bonded joints.

Presented as Paper 2001-1532 at the AIAA/ASME/ASCE/ASC/AHC 42nd Structures, Structural Dynamics, and Materials Conference, Seattle, WA, 16–19 April 2001; received 29 October 2004; revision received 28 February 2005; accepted for publication 28 February 2005.

*Professor, Department of Aerospace Engineering; yuceoglu@ae.metu.edu.tr.

†Ph.D., Department of Aerospace Engineering; vozerciyes@tai.com.tr.

Main Assumptions

In the theoretical analysis, the transverse shear deformations and the extensional, transverse, and rotatory moments of inertia are taken into account in the dissimilar, composite shallow shell adherends. Thus, an FSDST of Timoshenko–Mindlin (–Reissner) type (see Refs. 16–20) is employed in this study as a first approximation. There are several higher-order shear deformation shell theories in the literature. A recent one, given by Reddy and Liu,[21] completely eliminates the shear correction factors of the FSDSTs. An assessment of several theories and computational models may be found by Noor and Burton.[22] In the thin, yet flexible, adhesive layer, the adhesive transverse normal and shear stresses are included in the analysis.

The geometric characteristrics and the general configuration of the bonded single-lap joints in composite, shallow circular cylindrical shells or shell panels are presented in Fig. 1a. The longitudinal cross section or the longitudinal cut of the composite lap joint system is shown in Fig. 1b. The coordinate system is presented in both Figs. 1a and 1b. The material directions of the dissimilar, orthotropic, shallow shell adherends coincide with the principle curvatures of the shell elements. The sign convention for the stress resultants are according to the coordinate system in Fig. 1a for shell adherends and are based on the elasticity theory sign convention for stresses.

The shallow shell adherends (or shear diaphragm) are simply supported at edges $\varphi = 0, \varphi_0$. However, the other two opposite edges of the shallow shell or panel system in the x direction may have arbitrary support conditions. As shown in Fig. 1a, the shell elements are assumed to be made of two dissimilar, orthotropic materials. The damping effects in the shell elements and in the adhesive layer will be neglected in this study. The position of the single lap joint or the overlap region is at midcenter of the composite shell system.

Theoretical Formulation and Governing Differential Equations

In the theoretical formulation, taking into account the present method of solution, the shallow shell single lap joint system is divided into three parts (I–III) in the x direction as shown in Fig. 1b. As it will be seen later, this approach facilitates the solution of the lap joint problem under consideration. In the part I region, the dynamic equations of shallow shells with a thin adhesive layer in-between, the stress resultant-displacement expressions, and the orthotropic constitutive equations can be combined in a matrix form.

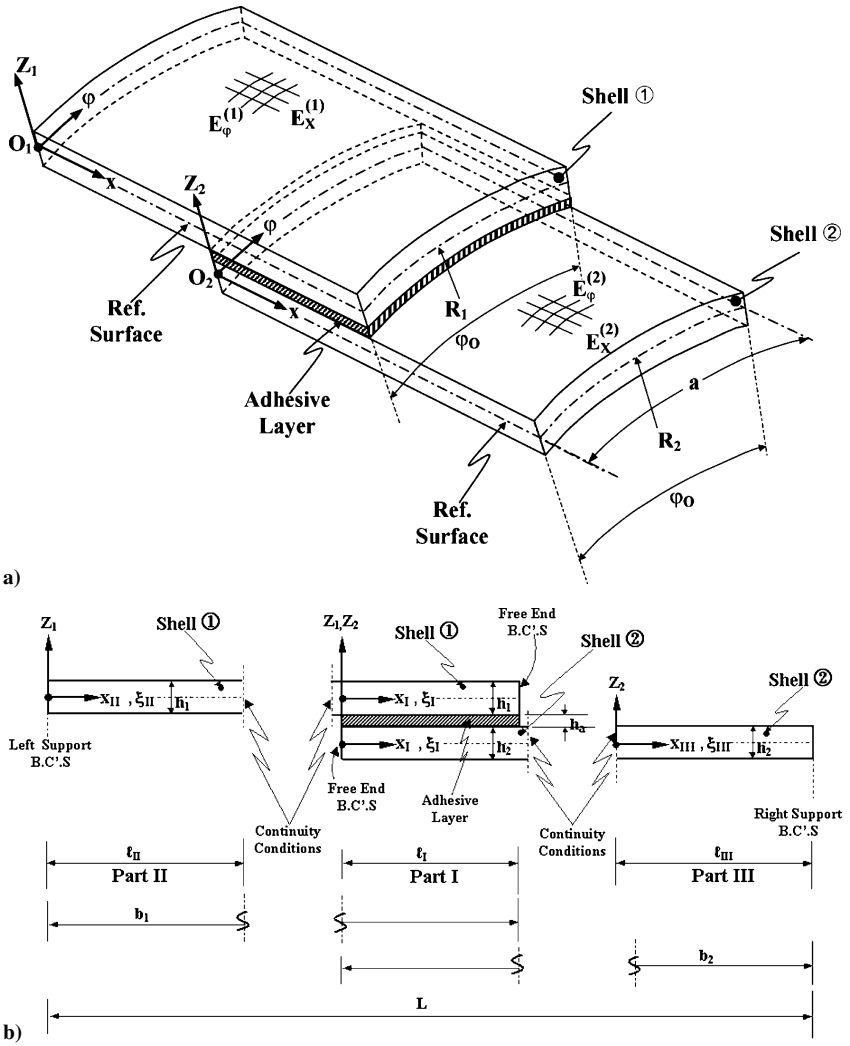

Fig. 1 General configuration, longitudinal cross section, and coordinate system of lap joint.

In the part I region (overlap region with two-layer shell and adhesive layer in-between),

$$\frac{\partial}{\partial \boldsymbol{x}_{\mathrm{I}}}\begin{Bmatrix}\boldsymbol{Z}^{(1)}\\ \boldsymbol{Z}^{(2)}\end{Bmatrix}=\left[\boldsymbol{C}\left(\frac{\partial}{\partial\varphi},\frac{\partial^2}{\partial\varphi^2},\frac{\partial^2}{\partial \boldsymbol{t}^2},\ldots\right)\right]\begin{Bmatrix}\boldsymbol{Z}^{(1)}\\ \boldsymbol{Z}^{(2)}\end{Bmatrix}\qquad(0<x_{\mathrm{I}}<\ell_{\mathrm{I}})\quad(1)$$

In the part II region (single-layer upper shell),

$$\frac{\partial}{\partial \boldsymbol{x}_{\mathrm{II}}}\left\{\boldsymbol{Z}^{(1)}\right\}=\left[\boldsymbol{D}\left(\frac{\partial}{\partial\varphi},\frac{\partial^2}{\partial\varphi^2},\frac{\partial^2}{\partial \boldsymbol{t}^2},\ldots\right)\right]\left\{\boldsymbol{Z}^{(1)}\right\}\qquad(0<x_{\mathrm{II}}<\ell_{\mathrm{II}})\quad(2)$$

In the part III region (single-layer lower shell),

$$\frac{\partial}{\partial \boldsymbol{x}_{\mathrm{III}}}\left\{\boldsymbol{Z}^{(2)}\right\}=\left[\boldsymbol{E}\left(\frac{\partial}{\partial\varphi},\frac{\partial^2}{\partial\varphi^2},\frac{\partial^2}{\partial \boldsymbol{t}^2},\ldots\right)\right]\left\{\boldsymbol{Z}^{(2)}\right\}\qquad(0<x_{\mathrm{III}}<\ell_{\mathrm{III}})\quad(3)$$

where the fundamental dependent variables of the problem can be written in a column matrix form as

$$\left\{\boldsymbol{Z}^{(i)}\right\}=\begin{Bmatrix}\boldsymbol{u}^{(i)},\boldsymbol{v}^{(i)},\boldsymbol{w}^{(i)},\beta_x^{(i)},\beta_\varphi^{(i)};\\ \boldsymbol{N}_{xx}^{(i)},\boldsymbol{N}_{x\varphi}^{(i)},\boldsymbol{M}_{xx}^{(i)},\boldsymbol{M}_{x\varphi}^{(j)},\bar{\boldsymbol{Q}}_{xz}^{(i)}\end{Bmatrix}^T\qquad(i=1,2)\qquad(4)$$

which contains the displacements, the angles of rotation, and the stress resultants appearing at any $x=$ constant.

The adhesive-layer stresses are considered as the surface loads acting on the upper and lower shallow shell adherends. Thus, they are included in the formulation. In this way, the shallow shells are coupled by means of the adhesive layer.

The nondimensionalizations of Eqs. (1–3) are now considered. For this purpose, ρ_2, h_2, R_2, $\boldsymbol{B}_{11}^{(2)}$, φ_0 are chosen as the reference parameters. Then, the dimensionless quantities are given as follows.

The dimensionless coordinates, in part I are

$$\xi_{\mathrm{I}}=\boldsymbol{x}_{\mathrm{I}}/\ell_{\mathrm{I}},\qquad \bar{\varphi}=\varphi/\varphi_0\qquad(5a)$$

in part II are

$$\xi_{\mathrm{II}}=\boldsymbol{x}_{\mathrm{II}}/\ell_{\mathrm{II}},\qquad \bar{\varphi}=\varphi/\varphi_0\qquad(5b)$$

and in part III are

$$\xi_{\mathrm{III}}=\boldsymbol{x}_{\mathrm{III}}/\ell_{\mathrm{II}},\qquad \bar{\varphi}=\varphi/\varphi_0\qquad(5c)$$

The dimensionless parameters related to the densities and the geometry of the system are

$$\bar{\rho}=\rho_1/\rho_2,\qquad \bar{\boldsymbol{h}}_a=\boldsymbol{h}_a/\boldsymbol{h}_2,\qquad \bar{\boldsymbol{R}}=\boldsymbol{R}_1/\boldsymbol{R}_2,\qquad \bar{\boldsymbol{h}}=\boldsymbol{h}_1/\boldsymbol{h}_2$$
$$\bar{\boldsymbol{b}}_{\mathrm{I}}=\boldsymbol{b}_1/\boldsymbol{R}_2,\qquad \bar{\boldsymbol{b}}_{\mathrm{II}}=\boldsymbol{b}_2/\boldsymbol{R}_2\qquad(6)$$

The dimensionless parameters involving the shallow shells and the adhesive layer elastic constants are

$$\bar{\boldsymbol{B}}_{jk}^{(i)} = \boldsymbol{B}_{jk}^{(i)} \big/ \boldsymbol{B}_{11}^{(2)} \qquad (i = 1, 2, \qquad j, k = 1, 2)$$

$$\bar{\boldsymbol{B}}_{\ell\ell}^{(i)} = \boldsymbol{B}_{\ell\ell}^{(i)} \big/ \boldsymbol{B}_{11}^{(2)} \qquad (i = 1, 2, \qquad \ell = 4, 5, 6)$$

$$\bar{\boldsymbol{G}}_a = \boldsymbol{G}_a \big/ \boldsymbol{B}_{11}^{(2)}, \qquad \bar{\boldsymbol{E}}_a = \boldsymbol{E}_a \big/ \boldsymbol{B}_{11}^{(2)} \tag{7}$$

The dimensionless natural frequency (or the circular frequency) of the entire shallow shell system are

$$\bar{\omega}_{mn} = \frac{\rho_2 \boldsymbol{R}^{\frac{7}{2}} \omega_{mn}^2}{\boldsymbol{h}_2^{\frac{3}{2}} \boldsymbol{B}_{11}^{(2)}} \qquad (m, n = 1, 2, 3, \ldots)$$

$$\bar{\Omega} = \bar{\omega}_{mn} \tag{8}$$

The two-layer shallow shell system in part I (or overlap region) (and also the entire lap joint system) along $\varphi = 0$, φ_0 is simply (or shear diaphragm) supported. At $x = 0, L$ along the other two edges in the x direction, the boundary conditions are arbitrary. Then, the classical Levy's solution may be assumed in Fourier series in the φ direction:

$$\boldsymbol{u}^{(i)} = \boldsymbol{h}_2 \sum_{m=1}^{\infty}\sum_{n=1}^{\infty} \bar{\boldsymbol{U}}_{mn}^{(i)}(\xi) \sin\left(\frac{\boldsymbol{n}\pi \boldsymbol{R}_i \varphi}{\boldsymbol{a}_i}\right) e^{j\omega_{mn}t}$$

$$\boldsymbol{v}^{(i)} = \boldsymbol{h}_2 \sum_{m=1}^{\infty}\sum_{n=1}^{\infty} \bar{\boldsymbol{V}}_{mn}^{(i)}(\xi) \cos\left(\frac{\boldsymbol{n}\pi \boldsymbol{R}_i \varphi}{\boldsymbol{a}_i}\right) e^{j\omega_{mn}t}$$

$$\boldsymbol{w}^{(i)} = \boldsymbol{h}_2 \sum_{m=1}^{\infty}\sum_{n=1}^{\infty} \bar{\boldsymbol{W}}_{mn}^{(i)}(\xi) \sin\left(\frac{\boldsymbol{n}\pi \boldsymbol{R}_i \varphi}{\boldsymbol{a}_i}\right) e^{j\omega_{mn}t}$$

$$(0 < \xi < 1 \qquad i = 1, 2)$$

$$\beta_x^{(i)} = \sum_{m=1}^{\infty}\sum_{n=1}^{\infty} \bar{\beta}_{xmn}^{(i)}(\xi) \sin\left(\frac{\boldsymbol{n}\pi \boldsymbol{R}_i \varphi}{\boldsymbol{a}_i}\right) e^{j\omega_{mn}t}$$

$$\beta_\varphi^{(i)} = \sum_{m=1}^{\infty}\sum_{n=1}^{\infty} \bar{\beta}_{\varphi mn}^{(i)}(\xi) \cos\left(\frac{\boldsymbol{n}\pi \boldsymbol{R}_i \varphi}{\boldsymbol{a}_i}\right) e^{j\omega_{mn}t} \tag{9a}$$

where the arc length on the middle surface is $\boldsymbol{a}_i = \boldsymbol{R}_i \varphi_0$, $i = 1, 2$ indicates the upper and lower shells, respectively, and the overbars indicate the dimensionless displacements and the angles of rotation. In Eq. (9), $j = \sqrt{-1}$ and ω_{mn} is the dimensional natural (or circular frequency) of the entire system.

Similarly, the appropriate dimensionless expressions can be written for the stress resultants appearing in Eq. (4):

$$\boldsymbol{N}_{xx}^{(i)} = \frac{\boldsymbol{h}_2^4 \boldsymbol{B}_{11}^{(2)}}{\boldsymbol{R}_2^3} \sum_{m=1}^{\infty}\sum_{n=1}^{\infty} \bar{\boldsymbol{N}}_{xxmn}^{(i)}(\xi) \sin\left(\frac{\boldsymbol{n}\pi \boldsymbol{R}_i \varphi}{\boldsymbol{a}_i}\right) e^{j\omega_{mn}t}$$

$$\boldsymbol{N}_{\varphi\varphi}^{(i)} = \frac{\boldsymbol{h}_2^4 \boldsymbol{B}_{11}^{(2)}}{\boldsymbol{R}_2^3} \sum_{m=1}^{\infty}\sum_{n=1}^{\infty} \bar{\boldsymbol{N}}_{\varphi\varphi mn}^{(i)}(\xi) \sin\left(\frac{\boldsymbol{n}\pi \boldsymbol{R}_i \varphi}{\boldsymbol{a}_i}\right) e^{j\omega_{mn}t}$$

$$\boldsymbol{N}_{x\varphi}^{(i)} = \frac{\boldsymbol{h}_2^4 \boldsymbol{B}_{11}^{(2)}}{\boldsymbol{R}_2^3} \sum_{m=1}^{\infty}\sum_{n=1}^{\infty} \bar{\boldsymbol{N}}_{x\varphi mn}^{(i)}(\xi) \cos\left(\frac{\boldsymbol{n}\pi \boldsymbol{R}_i \varphi}{\boldsymbol{a}_i}\right) e^{j\omega_{mn}t}$$

$$\boldsymbol{M}_{xx}^{(i)} = \frac{\boldsymbol{h}_2^5 \boldsymbol{B}_{11}^{(2)}}{\boldsymbol{R}_2^3} \sum_{m=1}^{\infty}\sum_{n=1}^{\infty} \bar{\boldsymbol{M}}_{xxmn}^{(i)}(\xi) \sin\left(\frac{\boldsymbol{n}\pi \boldsymbol{R}_i \varphi}{\boldsymbol{a}_i}\right) e^{j\omega_{mn}t}$$

$$\boldsymbol{M}_{\varphi\varphi}^{(i)} = \frac{\boldsymbol{h}_2^5 \boldsymbol{B}_{11}^{(2)}}{\boldsymbol{R}_2^3} \sum_{m=1}^{\infty}\sum_{n=1}^{\infty} \bar{\boldsymbol{M}}_{\varphi\varphi mn}^{(i)}(\xi) \sin\left(\frac{\boldsymbol{n}\pi \boldsymbol{R}_i \varphi}{\boldsymbol{a}_i}\right) e^{j\omega_{mn}t}$$

$$\boldsymbol{M}_{x\varphi}^{(i)} = \frac{\boldsymbol{h}_2^5 \boldsymbol{B}_{11}^{(2)}}{\boldsymbol{R}_2^3} \sum_{m=1}^{\infty}\sum_{n=1}^{\infty} \bar{\boldsymbol{M}}_{x\varphi mn}^{(i)}(\xi) \cos\left(\frac{\boldsymbol{n}\pi \boldsymbol{R}_i \varphi}{\boldsymbol{a}_i}\right) e^{j\omega_{mn}t}$$

$$\boldsymbol{Q}_{xz}^{(i)} = \frac{\boldsymbol{h}_2^4 \boldsymbol{B}_{11}^{(2)}}{\boldsymbol{R}_2^3} \sum_{m=1}^{\infty}\sum_{n=1}^{\infty} \bar{\boldsymbol{Q}}_{xzmn}^{(i)}(\xi) \sin\left(\frac{\boldsymbol{n}\pi \boldsymbol{R}_i \varphi}{\boldsymbol{a}_i}\right) e^{j\omega_{mn}t}$$

$$(0 < \xi < 1 \qquad i = 1, 2)$$

$$\boldsymbol{Q}_{\varphi z}^{(i)} = \frac{\boldsymbol{h}_2^4 \boldsymbol{B}_{11}^{(2)}}{\boldsymbol{R}_2^3} \sum_{m=1}^{\infty}\sum_{n=1}^{\infty} \bar{\boldsymbol{Q}}_{\varphi zmn}^{(i)}(\xi) \cos\left(\frac{\boldsymbol{n}\pi \boldsymbol{R}_i \varphi}{\boldsymbol{a}_i}\right) e^{j\omega_{mn}t} \tag{9b}$$

When the dimensionless displacements, angles of rotation, and dimensionless stress resultants from Eq. (9) are inserted into Eq. (1) and similar expressions valid in part II are substituted into Eqs. (2) and (3), then a reduced set of equations is obtained. Hence, the dimensionless governing system of ordinary differential equations in the state vector form are as follows.

In part I (two-layer shell and in-between adhesive layer),

$$\frac{\mathrm{d}}{\mathrm{d}\xi_{\mathrm{I}}} \begin{Bmatrix} \bar{\boldsymbol{Z}}_{mn}^{(1)} \\ \bar{\boldsymbol{Z}}_{mn}^{(2)} \end{Bmatrix} = \begin{bmatrix} \bar{\boldsymbol{C}}_{11} & \bar{\boldsymbol{C}}_{12} \\ \bar{\boldsymbol{C}}_{21} & \bar{\boldsymbol{C}}_{22} \end{bmatrix} \begin{Bmatrix} \bar{\boldsymbol{Z}}_{mn}^{(1)} \\ \bar{\boldsymbol{Z}}_{mn}^{(2)} \end{Bmatrix}$$

$$\begin{cases} (0 \le \xi_{\mathrm{I}} < 1) & \text{(upper shell)} \\ (0 < \xi_{\mathrm{I}} \le 1) & \text{(lower shell)} \end{cases} \tag{10}$$

In part II (single-layer upper shell),

$$\frac{\mathrm{d}}{\mathrm{d}\xi_{\mathrm{II}}} \left\{\bar{\boldsymbol{Z}}_{mn}^{(1)}\right\} = [\bar{\boldsymbol{\mathcal{D}}}] \left\{\bar{\boldsymbol{Z}}_{mn}^{(1)}\right\} \qquad (0 < \xi_{\mathrm{II}} \le 1) \tag{11}$$

In part III (single-layer lower shell),

$$\frac{\mathrm{d}}{\mathrm{d}\xi_{\mathrm{III}}} \left\{\bar{\boldsymbol{Z}}_{mn}^{(2)}\right\} = [\bar{\boldsymbol{\mathcal{E}}}] \left\{\bar{\boldsymbol{Z}}_{mn}^{(2)}\right\} \qquad (0 \le \xi_{\mathrm{III}} < 1) \tag{12}$$

where the dimensionless column matrix or the state vector $\{\bar{\boldsymbol{Z}}_{mn}^{(i)}\}$ is now

$$\left\{\bar{\boldsymbol{Z}}_{mn}^{(i)}\right\} = \left\{ \begin{matrix} \bar{\boldsymbol{U}}_{mn}^{(i)}, \bar{\boldsymbol{V}}_{mn}^{(i)}, \bar{\boldsymbol{W}}_{mn}^{(i)}, \bar{\beta}_{mnx}^{(i)}, \bar{\beta}_{mn\varphi}^{(i)}; \\ \bar{\boldsymbol{N}}_{mnxx}^{(i)}, \bar{\boldsymbol{N}}_{mnx\varphi}^{(i)}, \bar{\boldsymbol{M}}_{mnxx}^{(i)}, \bar{\boldsymbol{M}}_{mnx\varphi}^{(i)}, \bar{\boldsymbol{Q}}_{mnxz}^{(i)} \end{matrix} \right\}^T$$

$$(i = 1, 2) \tag{13}$$

which includes all of the dimensionless fundamental dependent variables of the problem. Equations (10) are given in open form in terms of the dimensionless fundamental dependent variables as are Eqs. (A1–A10) in Appendix A.

The first-order system of the governing ordinary differential equations (10–12) with the continuity conditions and the boundary conditions where appropriate constitute a two-point boundary value problem. Because the coefficient matrices in Eqs. (10–12) include $\bar{\omega}_{mn}$, these equations can be integrated numerically once the dimensionless natural frequency $\bar{\omega}_{mn}$ is obtained for a given particular case.

Solution Method and Numerical Procedure

The reduced systems of the governing differential equations (10–12) as given in the state vector form are now recast into a special form suitable for the method of solution called the modified transfer matrix method (with interpolation polynomials). This solution procedure is a further extension of the method developed by the present authors.[10–15] An earlier and simpler version is given by Yuceoglu et al.[23]

The modified transfer matrix method (with interpolation polynomials) is, essentially, a semi-analytical and numerical technique that combines the classical Lévy's method, the integrating matrix method, and the transfer matrix method for continuous systems. It is a very efficient and accurate procedure that can be easily used for a certain class of two-point boundary and initial value problems in plates and shells.

In the following development, the main steps of the present solution method will be briefly explained. As an initial step, the governing system of ordinary differential equations (10–12) are discretized.

This is accomplished by discretizing the dimensionless fundamental dependent variables and the coefficient matrices in Eqs. (10–12) with respect to ξ_{I}, ξ_{II}, and ξ_{III}, respectively. For this purpose, parts I–III, shown in Fig. 1b are divided into sufficient number of segments along the ξ_{I}, ξ_{II}, and ξ_{III} directions. Then the governing differential equations are premultiplied by the appropriate global integrating matrices $[\mathcal{L}]$, which include 20 square integrating submatrices $[\ell]$ of dimensions $(20k_1 \times 20k_1)$. Here, k_1 is the number of discretizing points along the ξ_{I} direction in part I. These operations yield the following equations (see also Appendix B).

In part I (two-layer shallow shell and adhesive layer),

$$\begin{Bmatrix} \dot{\bar{Z}}^{(1)}_{mn} \\ \dot{\bar{Z}}^{(2)}_{mn} \end{Bmatrix} - \begin{Bmatrix} \dot{\bar{Z}}^{(1)}_{\xi_{\mathrm{I}}=0} \\ \dot{\bar{Z}}^{(2)}_{\xi_{\mathrm{I}}=0} \end{Bmatrix} = [\mathcal{L}][\dot{\bar{\mathcal{C}}}] \begin{Bmatrix} \dot{\bar{Z}}^{(1)}_{mn} \\ \dot{\bar{Z}}^{(2)}_{mn} \end{Bmatrix} \qquad (0 \le \xi_{\mathrm{I}} \le 1) \quad (14)$$

where the overdot indicates the discretization of a particular matrix along the ξ_{I} direction and the overbar indicates the dimensionless terms. The subscript $(\xi_{\mathrm{I}} = 0)$ in the state vectors in Eq. (10) means that the state vectors are evaluated at the initial endpoint $\xi_{\mathrm{I}} = 0$ in part I. Note that state vectors are coupled by the adhesive layer (see Appendix C).

Equation (14) can be rearranged in such a way that a relation between the state vector at a general station ξ_{I} and a state vector at the initial endpoint $\xi_{\mathrm{I}} = 0$ is obtained. Then,

$$\begin{Bmatrix} \dot{\bar{Z}}^{(1)}_{mn} \\ \dot{\bar{Z}}^{(2)}_{mn} \end{Bmatrix} = [\dot{\mathcal{U}}] \begin{Bmatrix} \dot{\bar{Z}}^{(1)}_{\xi_{\mathrm{I}}=0} \\ \dot{\bar{Z}}^{(2)}_{\xi_{\mathrm{I}}=0} \end{Bmatrix}, \qquad [\dot{\mathcal{U}}] = ([\boldsymbol{I}] - [\mathcal{L}][\dot{\bar{\mathcal{C}}}])^{-1} \quad (15)$$

where $[\boldsymbol{I}]$ is the unit matrix and $[\dot{\mathcal{U}}]$ is the discretized version of the so-called modified transfer matrix along the ξ_{I} direction between a general or arbitrary station and the initial endpoint $\xi_{\mathrm{I}} = 0$. The discretized modified transfer matrix in Eq. (15) includes the integrating matrices (see also Appendix B). Thus, in part I, going from station to station along ξ_{I}, one can obtain a final relation between the state vectors at the initial endpoint $\xi_{\mathrm{I}} = 0$ and the final endpoint $\xi_{\mathrm{I}} = 1$. In the integrating matrices, the interpolation polynomials are employed. For convenience, the subscript mn in Eq. (15) is dropped.

In part I (two-layer shallow shell and adhesive layer),

$$\begin{Bmatrix} \dot{\bar{Z}}^{(1)}_{\xi_{\mathrm{I}}=1} \\ \dot{\bar{Z}}^{(2)}_{\xi_{\mathrm{I}}=1} \end{Bmatrix} = [\tilde{\mathcal{U}}]_{01} \begin{Bmatrix} \dot{\bar{Z}}^{(1)}_{\xi_{\mathrm{I}}=0} \\ \dot{\bar{Z}}^{(2)}_{\xi_{\mathrm{I}}=0} \end{Bmatrix}, \qquad [\tilde{\mathcal{U}}]_{01} = \begin{Bmatrix} \tilde{\mathcal{U}}_{1,1} & \tilde{\mathcal{U}}_{1,2} \\ \tilde{\mathcal{U}}_{2,1} & \tilde{\mathcal{U}}_{2,2} \end{Bmatrix}$$

$$(0 \le \xi_{\mathrm{I}} \le 1) \quad (16)$$

where $[\tilde{\mathcal{U}}_{i,j}]_{01}$, $i, j = 1, 2$ are partioned square matrices of (10×10) that explicitly include the dimensionless natural frequency parameter $\bar{\omega}_{mn}$. In Eq. (16), the subscript 01 indicates that the final form of the modified transfer matrix $[\tilde{\mathcal{U}}]_{01}$ transfers the state vector from the initial endpoint $\xi_{\mathrm{I}} = 0$ (or the initial station) to the final endpoint $\xi_{\mathrm{I}} = 1$ (or the final station). The end result of the discretization procedure of the state vectors, the coefficient matrices, and the final form of the modified transfer matrix, as shown in Eq. (16), are given in detail in Appendix B.

In a similar way, the expressions corresponding to the Eq. (16) with the appropriate final form of the modified transfer matrices can be obtained for parts II and III in terms of $[\tilde{\mathcal{V}}]_{01}$ and $[\tilde{\mathcal{W}}]_{01}$, respectively. After the substitution of the continuity conditions between parts I and II, similarly parts I and III (Fig. 1b) and the insertion of the support conditions in the x direction of the upper and the lower shallow shell elements, a matrix equation is obtained:

$$[\boldsymbol{C}_0(\bar{\omega}_{mn})]\{\boldsymbol{Z}_0\} = \{0\} \quad (17)$$

where the coefficient matrix $[\boldsymbol{C}_0]$ includes dimensionless natural frequecies $\bar{\omega}_{mn}$. Therefore, the determinant of the coefficient matrix yields the polynomial that has the natural frequencies as its roots (nontrivial solution). Thus, the determinant is

$$|\boldsymbol{C}_0(\bar{\omega}_{mn})| = 0 \quad (18)$$

The roots or the natural frequencies are

$$\bar{\Omega} = \bar{\omega}_{mn} \qquad (m, n = 1, 2, 3, \ldots)$$

$$\bar{\Omega}_1 < \bar{\Omega}_2 < \bar{\Omega}_3 < \cdots \quad (19)$$

where the dimensionless natural frequencies $\bar{\Omega}$ in Eq. (19) are sequenced or ordered according to their magnitudes as shown. Depending on the given n and the assigned m values and their magnitudes, the sequencing of the subscripts $1, 2, 3, \ldots$, in $\bar{\Omega}$ indicates first, second, third, ..., natural frequencies, respectively. Here, m is a dummy subscript, whereas n comes from the trigonometric series or rather from the classical Levy's solution.

Numerical Applications and Discussion

The preceding methodology for the theoretical analysis and the solution technique developed by the present authors is applied to the problem under study here. The method of solution is the relatively new modified transfer matrix method (with interpolation polynomials) developed and extended by Yuceoglu and Özerciyes[10–15] for some free-vibration problems of composite plates and/or shells. [Two other versions of the method, suitable for the sixth and higher frequencies, by the present authors are the modified transfer matrix method (with Chebyshev polynomials) and the modified transfer matrix method (with the eigenvalue approach), which will be reported later in another paper.]

Table 1 Material properties and dimensions[a]

Kevlar–epoxy, $i = 1$		Graphite–epoxy, $i = 2$		Soft adhesive layer		Hard adhesive layer	
Property	Value	Property	Value	Property	Value	Property	Value
$\boldsymbol{E}_x$	5.50 GPa	$\boldsymbol{E}_x$	11.71 GPa	$\boldsymbol{E}_a/\boldsymbol{B}^{(1)}_{11}$	1.0×10^{-5}	$\boldsymbol{E}_a/\boldsymbol{B}^{(1)}_{11}$	3.4×10^{-2}
$\boldsymbol{E}_\varphi$	76.0 GPa	$\boldsymbol{E}_\varphi$	137.8 GPa	$\boldsymbol{G}_a/\boldsymbol{B}^{(1)}_{11}$	1.0×10^{-5}	$\boldsymbol{G}_a/\boldsymbol{B}^{(1)}_{11}$	1.19×10^{-2}
$\boldsymbol{G}_{x\varphi}$	2.10 GPa	$\boldsymbol{G}_{x\varphi}$	5.51 GPa	$\boldsymbol{h}_a$	0.15×10^{-3} m	$\boldsymbol{h}_a$	0.15×10^{-3} m
$\boldsymbol{G}_{xz}$	1.50 GPa	$\boldsymbol{G}_{xz}$	2.50 GPa	ρ_a	Neglected	ρ_a	Neglected
$\boldsymbol{G}_{\varphi z}$	2.00 GPa	$\boldsymbol{G}_{\varphi z}$	3.00 GPa			$\boldsymbol{E}_a$	4.0 GPa
$\nu_{x\varphi}$	0.024	$\nu_{x\varphi}$	0.0213			$\boldsymbol{G}_a$	1.4 GPa
$\nu_{\varphi x}$	0.34	$\nu_{\varphi x}$	0.25				
ρ_2	1.3 g/cm^3	ρ_1	1.6 g/cm^3				
$\boldsymbol{h}_2 = \boldsymbol{h}_1 = \boldsymbol{h}$	0.007 m	$\boldsymbol{h}_1 = \boldsymbol{h}_2 = \boldsymbol{h}$	0.007 m				
b_1	1.0 m	b_2	1.0 m				
ℓ_{I}	0.3 m	$\boldsymbol{a}$	0.5 m				
		$\boldsymbol{L}$	1.7 m (const)				
		$\boldsymbol{R}$	1.0 m				

[a] $\boldsymbol{L}$ = Total length of lap joint system $= \boldsymbol{L} = \boldsymbol{b}_1 + \boldsymbol{b}_2 - \ell_{\mathrm{I}}$ (see also Fig. 1b).

For numerical calculations, the dissimilar orthotropic material and the geometric characteristics of the shallow cylindrical shell lap joint system are given in Table 1. For the shear correction factors κ_x^2 and κ_φ^2 in the present study, a constant based on Wittrick's work[24] is used, 0.822. The adhesive elastic layer constants for the hard and the soft adhesive cases are also included in Table 1. The hard adhesive elastic constants are from the actual adhesives and are realistic. The soft adhesive constants, however, are used only to simulate and calculate the effects of a soft (or considerably flexible) adhesive layer.

In this study, to see the influence of the hard and the soft adhesive layers, the mode shapes (and the corresponding natural frequencies) are calculated and presented in Figs. 2–4. The boundary conditions considered are typical and practical support conditions. Additionally, the effect of some important parameters on the natural frequencies and mode shapes are computed and presented in Figs. 5–10.

The boundary conditions for the upper and lower shallow shell adherends in Figs. 2–10 are the support conditions in the x direction only, and they read from left to right. Thus, the first two letters indicate the boundary conditions of the upper shell, followed by two letters indicating the support conditions of the lower shell. Then, the letters are F for free, C for clamped, and S for simple support (or shear diaphragm support), respectively.

Note that, although not presented here, the general appearance and the trend in mode shapes for the SFFS boundary conditions are found to be very similar to those of the CFFC case shown in Fig. 2. This is because the lap joint system under consideration is relatively long in the x direction. Hence, the simple support or the clamped support effects do not propagate enough to produce significantly different mode shapes. Therefore, only the mode shapes corresponding to the CFFC support conditions are shown here.

In Fig. 2, the mode shapes (with the corresponding natural frequencies), in the case of the CFFC boundary conditions are shown for the hard (left-hand side) and the soft (right-hand side) adhesive cases, respectively. In Figs. 2–4, shell 1 is Kevlar®–epoxy and shell 2 is graphite epoxy. The joint length $\ell_1 = 0.3$ m, $b_1 = b_2 = 1.0$ m, $L = 1.7$ m, $a = 0.5$ m, and $\ell_1/L = 0.176$. It can be seen from Fig. 2 that the general appearance and the trend in the mode shapes, in both

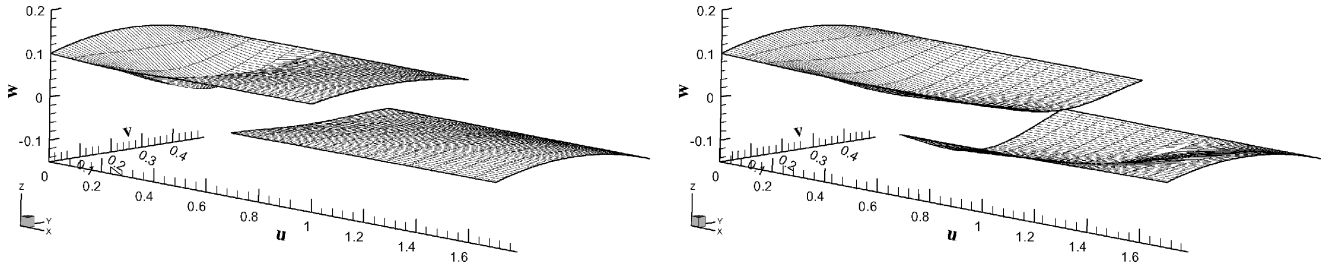

a) $\bar{\Omega}_1 = \bar{\omega}_{11} = 204.50$ first mode $\bar{\Omega}_1 = \bar{\omega}_{11} = 124.92$

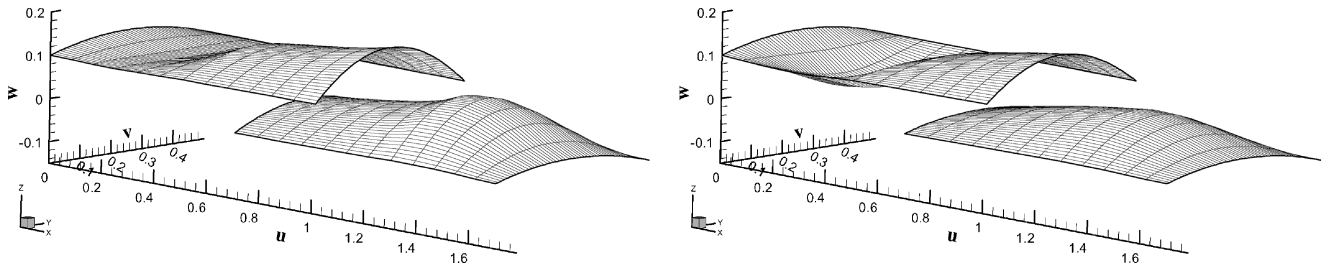

b) $\bar{\Omega}_2 = \bar{\omega}_{21} = 274.91$ second mode $\bar{\Omega}_2 = \bar{\omega}_{21} = 220.64$

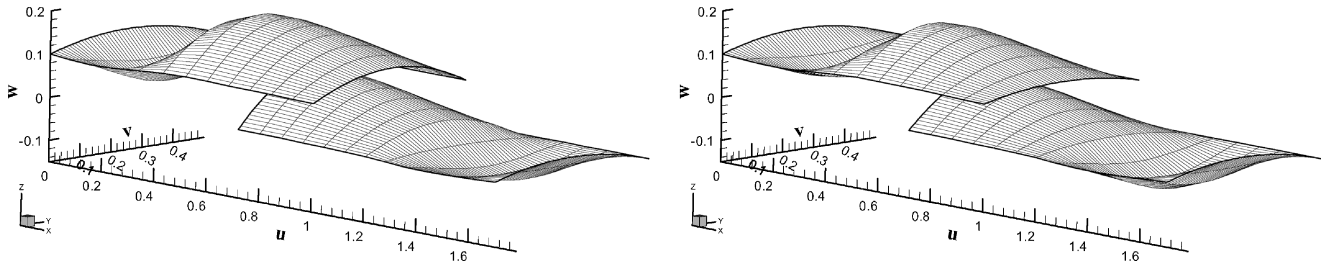

c) $\bar{\Omega}_3 = \bar{\omega}_{31} = 494.47$ third mode $\bar{\Omega}_3 = \bar{\omega}_{31} = 395.57$

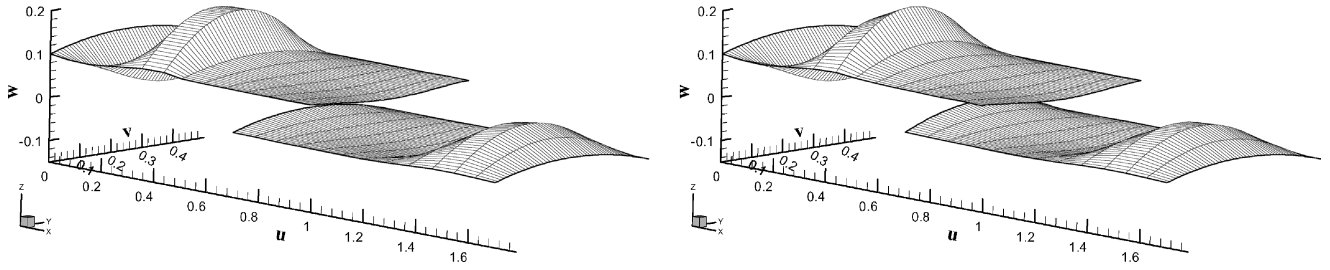

d) $\bar{\Omega}_4 = \bar{\omega}_{41} = 795.73$ fourth mode $\bar{\Omega}_4 = \bar{\omega}_{41} = 716.27$

Fig. 2 Mode shapes and natural frequencies: CFFC boundary conditions in the x direction.

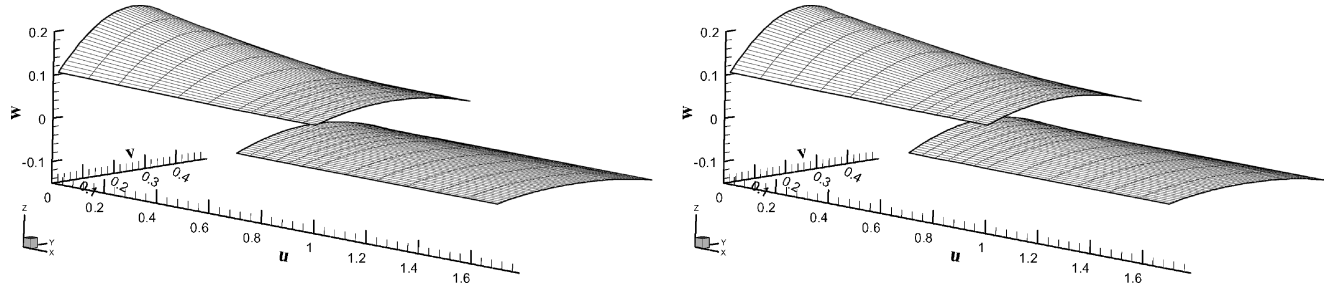

a) $\bar{\Omega}_1 = \bar{\omega}_{11} = 88.47$ first mode $\bar{\Omega}_1 = \bar{\omega}_{11} = 84.13$

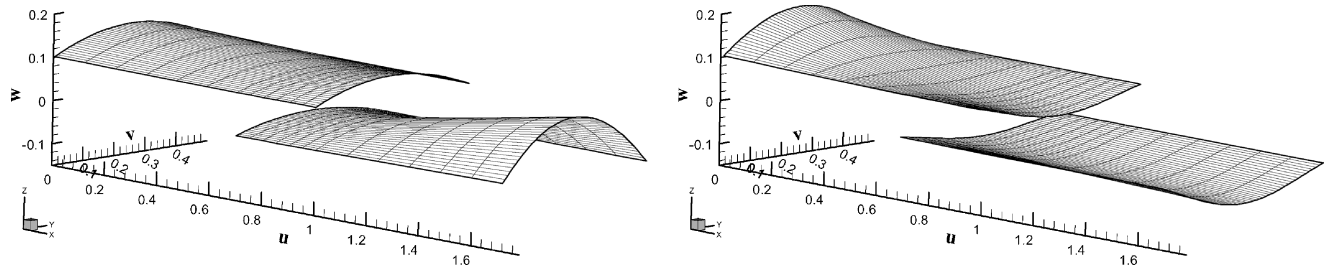

b) $\bar{\Omega}_2 = \bar{\omega}_{21} = 133.55$ second mode $\bar{\Omega}_2 = \bar{\omega}_{21} = 117.77$

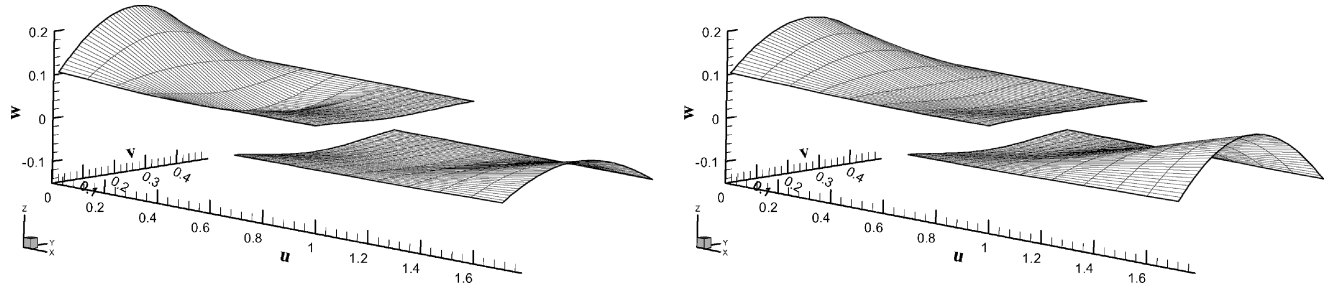

c) $\bar{\Omega}_3 = \bar{\omega}_{31} = 249.83$ third mode $\bar{\Omega}_3 = \bar{\omega}_{31} = 141.70$

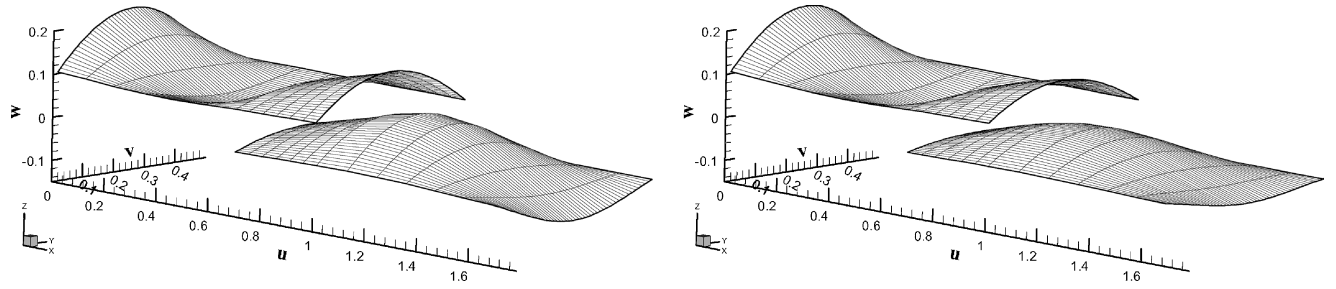

d) $\bar{\Omega}_4 = \bar{\omega}_{41} = 341.44$ fourth mode $\bar{\Omega}_4 = \bar{\omega}_{41} = 299.35$

Fig. 3 Mode shapes and natural frequencies: FFFF boundary conditions in the *x* direction.

hard and soft cases, are similar. However, because of the additional flexibility of the shell lap joint system with the soft adhesive, the natural frequencies are smaller.

In Fig. 3, the mode shapes (and the corresponding natural frequencies) for the FFFF support conditions are presented in the hard (left-hand side) and the soft (right-hand side) cases, respectively. It can be seen from Fig. 3, only the second modes are different in general appearance whereas the other modes seem to have similar shapes corresponding to both the hard and the soft adhesive cases. The natural frequencies, however, in the hard adhesive case are higher, as expected.

In Fig. 4, the mode shapes (and the corresponding natural frequencies), in the case of the CFFF support conditions, are presented for the hard (left-hand side) and the soft (right-hand side) adhesive cases, respectively. From the comparison of each mode, it can be observed that no similar trend occurs in the mode shapes for both the hard and the soft adhesive cases.

In Fig. 5, the dimensionless natural frequencies vs the joint length ratio $\ell_1/\boldsymbol{L}$ are plotted for the CFFC boundary conditions for the hard and the "soft" adhesive cases. (All other parameters remains the same as in Figs. 2–4.) In the hard adhesive case, as the overlap region increases so do the first three natural frequencies, although, rather gradually. However, in the fourth mode (Fig. 5), the frequencies increase at first, and then after the joint length ratio $\ell_1/\boldsymbol{L}$ reaches 0.7 value, they drop. This occurs in spite of the increasing length of the overlap or joint length region, which should actually create a stiffer structure, and so the increase, not the decrease, in the natural frequencies should be observed. To explain this phenomenon or contradiction, the fourth mode shapes corresponding to the joint length ratio $\ell_1/\boldsymbol{L}$ values of 0.6, 0.7, and 0.8 with CFFC conditions for the hard adhesive are shown in Fig. 6. Note from Fig. 6 that the comparison of the mode shapes corresponding to the joint length ratio $\ell_1/\boldsymbol{L} = 0.7$ and 0.8 can explain the frequency drop at 0.8. The narrow single-layer portions of the panel system at both ends no longer have separate half-waves. Instead, the very short or narrow length single-layer portions have half-waves together with the very stiff, two-layer overlap region. Thus, the frequency drop occurs. Also note that, as the joint length ratio $\ell_1/\boldsymbol{L}$ increases, the total

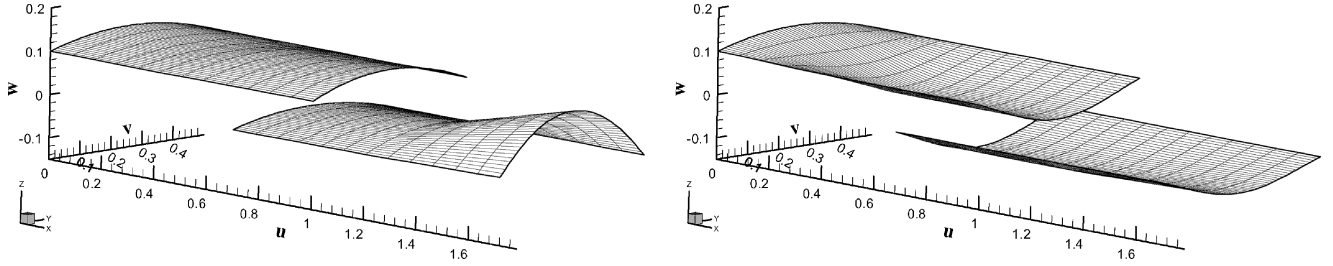

a) $\bar{\Omega}_1 = \bar{\omega}_{11} = 131.74$ first mode $\bar{\Omega}_1 = \bar{\omega}_{11} = 117.16$

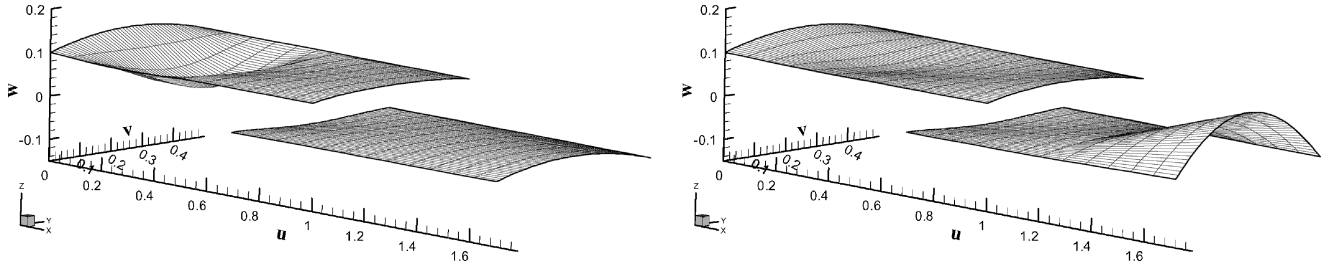

b) $\bar{\Omega}_2 = \bar{\omega}_{21} = 204.02$ second mode $\bar{\Omega}_2 = \bar{\omega}_{21} = 131.58$

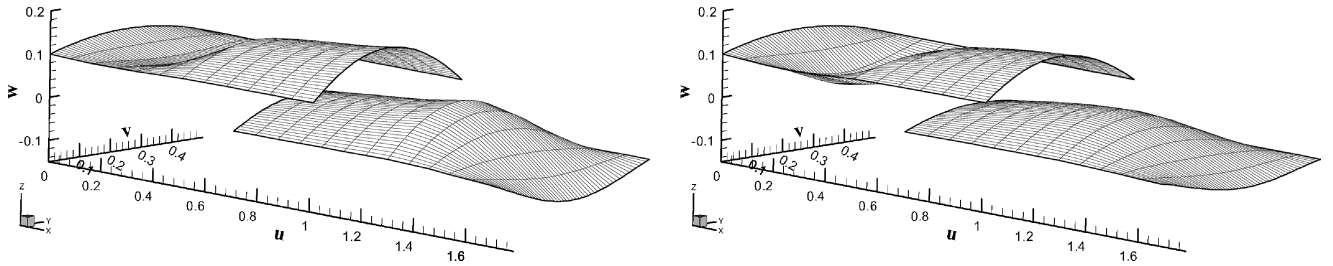

c) $\bar{\Omega}_3 = \bar{\omega}_{31} = 312.33$ third mode $\bar{\Omega}_3 = \bar{\omega}_{31} = 239.36$

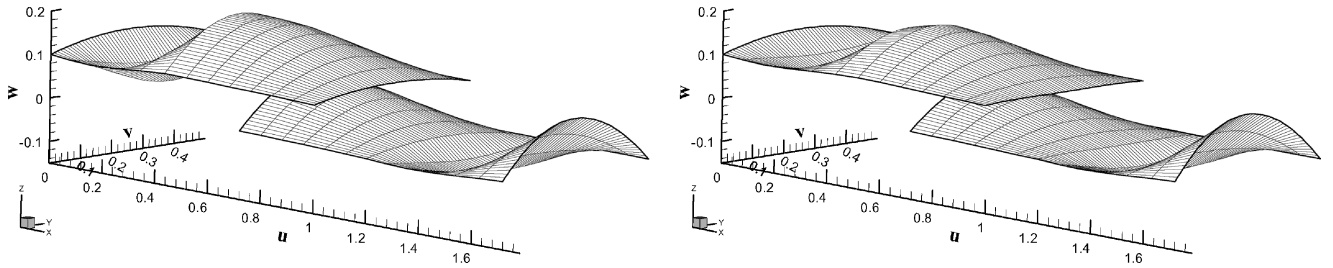

d) $\bar{\Omega}_4 = \bar{\omega}_{41} = 559.61$ fourth mode $\bar{\Omega}_4 = \bar{\omega}_{41} = 479.27$

Fig. 4 Mode shapes and natural frequencies: CFFF boundary conditions in the *x* direction.

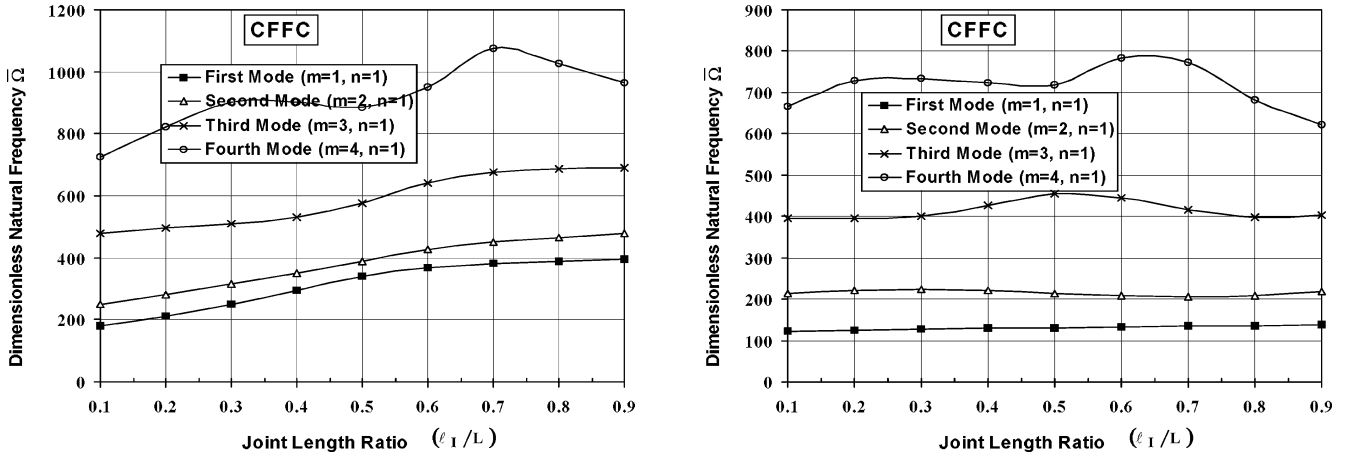

a) Hard adhesive b) Soft adhesive

Fig. 5 Natural frequency vs joint length ratio ℓ_1/L: CFFC.

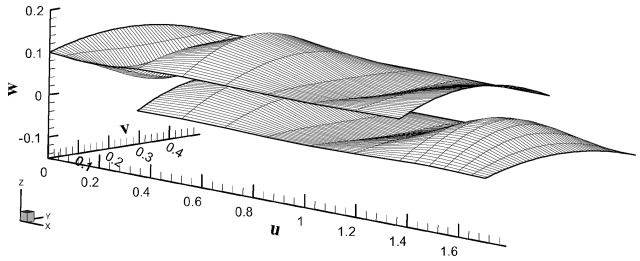

a) $\ell_1/L = 0.6$ m, $\ell_1 = 1.02$ m, $b_1 = b_2 = 1.36$ m, $\bar{\Omega}_4 = \bar{\omega}_{41} = 949.61$

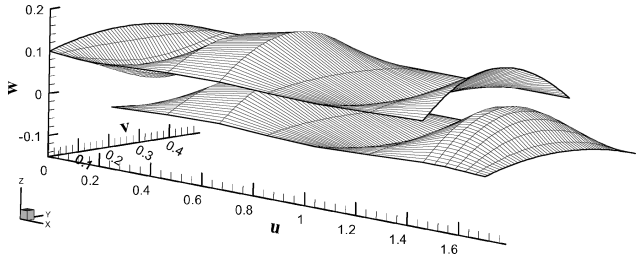

b) $\ell_1/L = 0.7$ m, $\ell_1 = 1.19$ m, $b_1 = b_2 = 1.45$ m, $\bar{\Omega}_4 = \bar{\omega}_{41} = 1075.87$

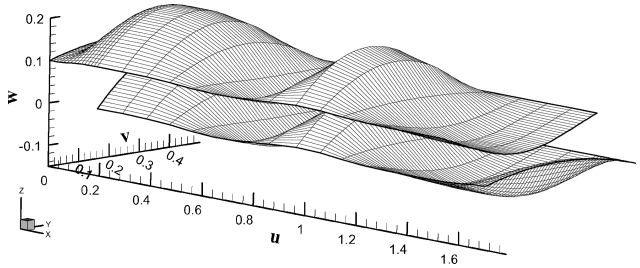

c) $\ell_1/L = 0.8$ m, $\ell_1 = 1.36$ m, $b_1 = b_2 = 1.53$ m, $\bar{\Omega}_4 = \bar{\omega}_{41} = 1028.04$

Fig. 6 Fourth mode shapes and natural frequencies: CFFC boundary conditions in the *x* direction.

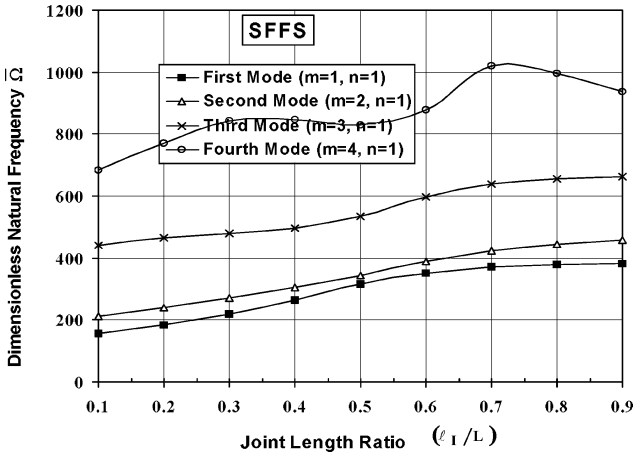

a) Hard adhesive

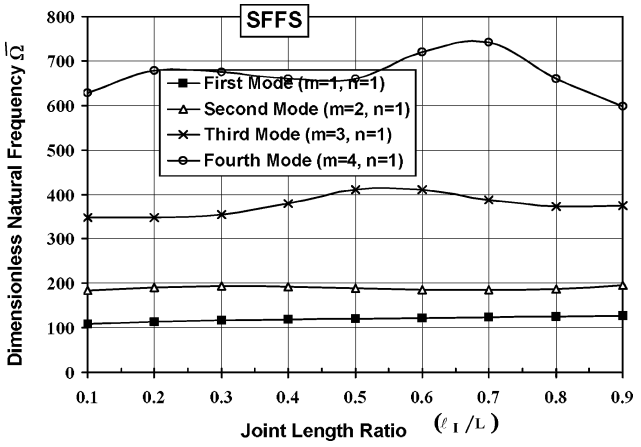

b) Soft adhesive

Fig. 7 Natural frequency vs joint length ratio ℓ_1/L: SFFS boundary conditions in the *x* direction.

mass of the system is increasing, too. This may also, additionally, cause a drop in frequencies.

Similar conclusions can be said about the fourth mode in Fig. 5 in the soft adhesive case for the similar CFFC conditions. Note that, in the case of the soft adhesive, both shallow shell adherends are relatively loosely connected. Thus, the overall system is very flexible and lightly constrained.

Similar observations can be made in Fig. 7, in which the natural frequencies vs the joint length ratio $\ell_1/\boldsymbol{L}$ are plotted for the hard and the soft adhesive cases. Figures 7a and 7b correspond to the SFFS support conditions. The comparison of Figs. 5 and 7 clearly indicates that the effect of the CFFC and the SFFS support conditions on the natural frequencies are somewhat similar (at least up to the fourth mode). The natural frequency curves have similar trends in both cases of support conditions.

The significant effect of some of the support conditions, in particular, the FFFF conditions on the natural frequencies can be seen in Fig. 8 corresponding to the hard and the soft adhesive cases. Comparison of Fig. 8 with Fig. 7 (and also with Fig. 5) indicates that the FFFF conditions create completely different natural frequency curves corresponding to the first four modes, as well as completely different mode shapes. Also, the trend in the frequencies for the hard and soft adhesive cases in Fig. 8 are very similar. Note that, in Fig. 8, as the joint length ratio $\ell_1/\boldsymbol{L}$ increases the natural frequencies go up slowly at first and, then, sharply for the third and especially for the fourth modes.

The influence of the various support conditions on the first natural frequencies (or on the fundamental frequencies) is also considered, and the results are presented in Fig. 9, corresponding to the hard and soft adhesive cases, respectively. Note that, as concluded before, the first natural frequency (or the fundamental frequency) curves for the CFFC and SFFS conditions are closely parallel to each other in both adhesive cases. Also, in the hard adhesive case, in Fig. 9, the fundamental frequency curves go up relatively sharply and linearly at first. Afterward, they start to flatten as the joint length ratio $\ell_1/\boldsymbol{L}$ reaches 0.8 for both the CFFC and SFFS support conditions. In Fig. 9, for the other less stiff or less constraining support conditions, the fundamental frequency curves are again parallel and close to each other. Also, for less stiff boundary conditions, the fundamental frequency increases very slowly, and after $\ell_1/\boldsymbol{L} = 0.7$, the increases are rather sharp.

In Fig. 9, for the soft adhesive case, the fundamental frequencies corresponding to the CFFC and SFFS conditions are almost linear and closely parallel each other. However, the slope of the frequency curves (or the rate of increase in frequencies) is very small. For the CFFF and SFFF conditions, the corresponding fundamental frequency curves are practically flat and almost coincide with each other. In the case of the FFFF support conditions (Fig. 9), the corresponding fundamental frequency curve is increasing gradually and is completely separate from other curves. One may conclude that, in the soft adhesive case, the fundamental frequencies corresponding to the CFFC, SFFS, CFFF, and SFFF conditions are close to each other and they all increase very slowly as the overlap region increases. Note that both shallow shell adherends are relatively stiff due to the shell curvatures and they are very loosely connected with the soft adhesive layer. Also, the mass of each adherend increases as the overlap region spreads. Thus, any sharp increases in fundamental frequencies can not be expected.

In Fig. 10, the natural frequencies of the first four modes vs the bending rigidity ratio $\boldsymbol{D}_{11}^{(1)}/\boldsymbol{D}_{11}^{(2)}$ are shown for the CFFC support conditions and for the hard and the soft adhesive cases, respectively. Here $\ell_1 = 0.3$ m, $b_1 = b_2 = 1.0$ m, and $a = 0.5$ m. As the bending rigidity ratio increases, the natural frequencies increase gradually. However, in both hard and soft cases, it can be seen that the effect

of the increases in the bending rigidity ratio $D_{11}^{(1)}/D_{11}^{(2)}$ on the natural frequencies is not as significantly large as can be expected. This may be explained as the consequence of the overly stiffening effect of the shell curvatures rather than the shell bending stiffnesses (even when the shell adherends are rather shallow shells). In Fig. 10, it can also be seen that the natural frequencies for the first two modes remain almost constant (or show very little increase) as the $D_{11}^{(1)}/D_{11}^{(2)}$ ratio increases.

Although not shown here, the natural frequencies vs the elastic constants of adhesive layer are also studied (up to the fifth mode). It was found that the adhesive shear modulus G_a more significantly influences the natural frequencies in comparison with the Young modulus E_a.

The problem of free vibrations of bonded single lap joints in composite shallow circular cylindrical shells or shell panels is formulated in the state-vector form and is solved by making use of the modified transfer matrix method (MTMM) with interpolation polynomials or with Chebyshev polynomials.

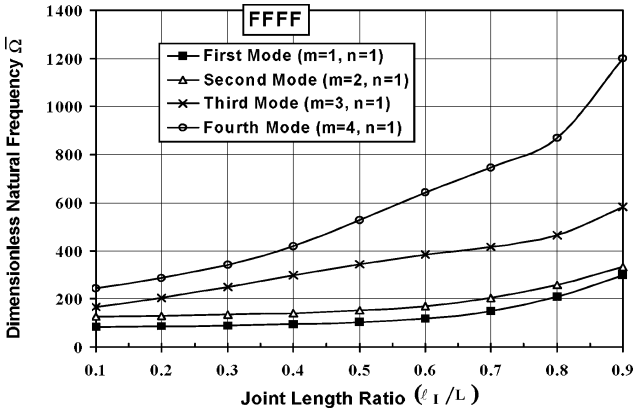

a) Hard adhesive

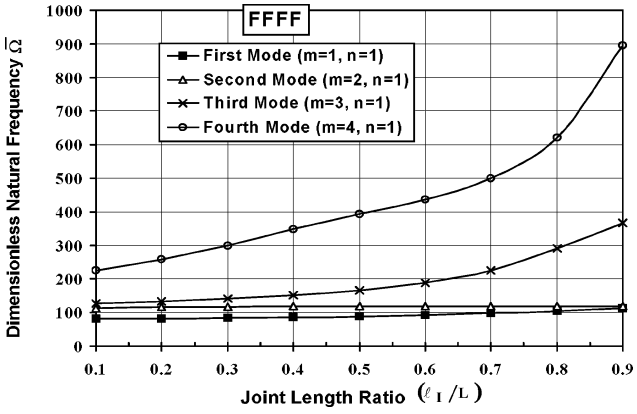

b) Soft adhesive

Fig. 8 Natural frequency vs joint length ratio ℓ_I/L: FFFF boundary conditions in the x direction.

To the best of the authors' knowledge, there are no available solutions for free vibrations of lap joints in shallow or full circular cylindrical shells. Therefore, the accuracy of this relatively new semi-analytical and numerical procedure is checked against the analytical solution available and given by Soedel[18,19] for the axisymmetric vibrations of isotropic one-layer full circular cylindrical shells. The comparison of the numerical results for the natural frequencies up to the sixth mode obtained by Soedel and by the present authors shows exceptionally good results and correlations. (The percentage errors in the frequencies obtained by the present method with interpolation polynomials are around $2.0 \times 10^{-6}\%$ up to the fifth mode, and it is around $3.5 \times 10^{-1}\%$ after that. The natural frequencies obtained by the present method with Chebyshev polynomials are much better and very accurate.) These results are presented in Table 2. In

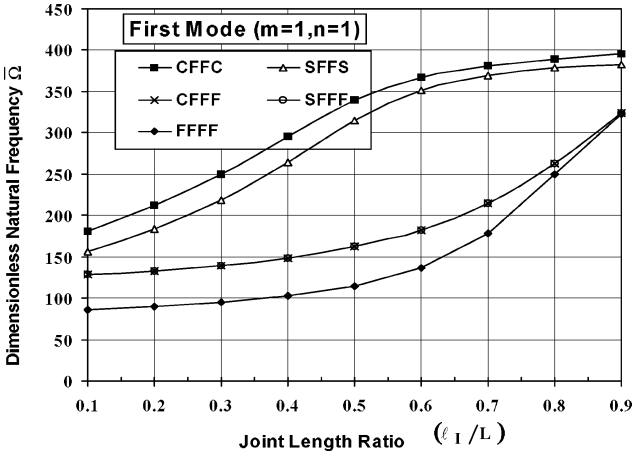

a) Hard adhesive

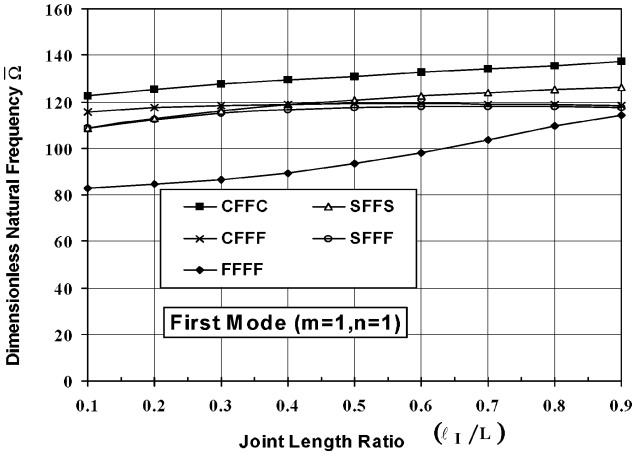

b) Soft adhesive

Fig. 9 Fundamental natural frequency vs joint length ratio ℓ_I/L: various boundary conditions in the x direction.

Table 2 Comparisons of natural frequencies in full circular cylindrical shells[a]

	Natural frequencies		
Mode	Analytical solution (FSDST)[18,19]	Chebyshev polynomials of the first kind, $N = 21$	MTMM, sixth-degree interpolation polynomial and Newton's forward difference formula
1st ($m = 1$)	49,852.518	49,852.518	49,852.520
2nd ($m = 2$)	51,054.226	51,054.226	51,054.291
3rd ($m = 3$)	51,558.34	51,558.340	51,559.779
4th ($m = 4$)	52,565.55	52,565.550	52,562.852
5th ($m = 5$)	54,556.186	54,556.185	54,363.748
6th ($m = 6$)	57,966.427	57,966.426	57,377.472

[a]Material steel, $E = 206.00$ GPa, $\nu = 0.3$, $\rho = 7850$ kg/m^3, $R = 0.1$ m, $L = 0.2$ m, $h = 0.002$ m, simple support at $x = 0, L$.

Table 3 Comparisons of natural frequencies in shallow circular cylindrical shells[a]

Mode	Analytical solution CLTST[25]	FSDST, MTMM
1st	1274.678	1251.89
2nd	2827.858	2800.33
3rd	4051.465	3939.62
4th	5098.712	4836.82

[a]Material aluminum, $E = 72.69$ GPa, $\nu = 0.313$, $\rho = 2796$ kg/m^3, $R = 1.0$ m, $L = 1.0$ m, $\varphi_0 = 0.5$ rad, $h = 0.01$ m, simple support at $x = 0, L$. CLTST, classical shell theory.

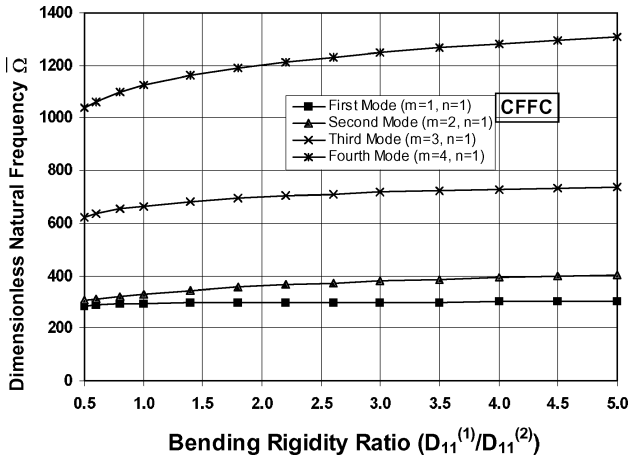

a) Hard adhesive

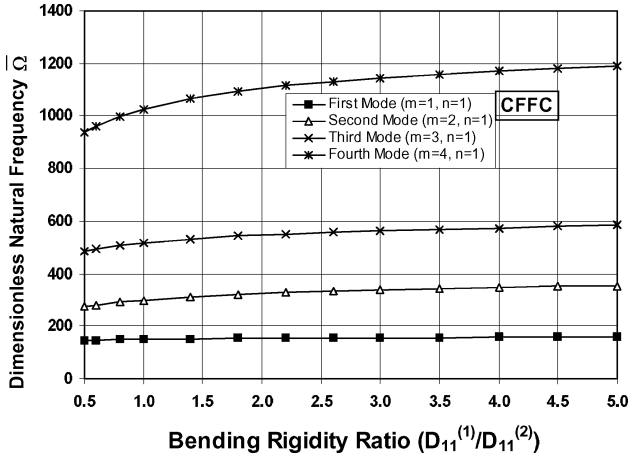

b) Soft adhesive

Fig. 10 Natural frequency vs bending rigidity ratio $D_{11}^{(1)}/D_{11}^{(2)}$ (shell 1 = varies, shell 2 = Kevlar–epoxy).

addition, the numerical results obtained for shallow circular cylindrical shells (CLTST) by Warburton[25] and by the present method for shallow circular cylindrical shells (FSDST) are shown in Table 3. As expected the FSDST yields lower frequencies than Warburton's results,[25] in which the effects of the in-plane and rotary moments of inertia are not included in the CLTST dynamic equations (same as with Vlasov's equations).

Conclusions

On the basis of the preceeding numerical results, the main conclusions are as follows:

1) The present formulation and the solution technique are very efficient and accurate. They can further be extended to other similar vibration problems of shallow or full composite cylindrical shells.

2) The main limitation is that the two opposite edges of the shallow shell lap joint system must have simple (or shear diaphragm) support, whereas the other two opposite edge conditions may be arbitrary.

3) The hard and the soft adhesive layer elastic constants significantly influence the natural frequencies for the same support conditions. However, the general appearance of the mode shapes are similar for the same boundary condition.

4) Because of the shear deformable character of the shallow shell adherends, the adhesive shear modulus G_a (rather than the adhesive elastic modulus E_a) has a considerable effect on the natural frequencies.

5) In the hard adhesive case, the curves for the natural frequencies vs the joint length ratio ℓ_1/L have similar trends corresponding to the CFFC and the SFFS support conditions. However, in the fourth mode (and perhaps in higher modes), the natural frequency curve reaches its maximum value at $\ell_1/L = 0.7$, and then, the natural frequencies start decreasing.

6) In the soft adhesive case and with CFFC and SFFS boundary conditions, the curves for the natural frequencies vs the joint length ratio ℓ_1/L, yield similar conclusions.

7) For FFFF support conditions, however, the natural frequencies vs the joint length ratio ℓ_1/L are very different than those of CFFC and SFFS conditions, in both hard and soft adhesive cases.

8) The first (or the fundamental dimensionless frequencies) vs the joint length ratio ℓ_1/L have similar trends for CFFC and SFFS conditions for both hard and soft adhesive cases.

9) The effect of the bending rigidity ratio $D_{11}^{(1)}/D_{11}^{(2)}$ on the natural frequencies for the first two modes is not very significant regardless of hardness or softness of the adhesive layer.

10) The characteristic mode shapes of the shallow shell lap joint and the plate jont systems are very much different due to the stiffening effect of shell curvatures. (Also see Yuceoglu et al.[23])

Appendix A: Governing Differential Equations in Open Form

In the part I region with an adhesive layer based on the Timoshenko–Mindlin (Reissner)-type shallow shell theory (FSDST) first-order system equations are as follows.

The first-order system in dimensionless displacements and angles of rotation are

$$\frac{\mathrm{d}\bar{U}_{mn}^{(i)}}{\mathrm{d}\xi} = \left[\frac{h_2^2}{R_2^2}\frac{\bar{b}_i}{\bar{h}_i}\frac{1}{\bar{B}_{11}^{(i)}}\bar{N}_{xxmn}^{(i)} - \frac{\bar{B}_{12}^{(i)}}{\bar{B}_{11}^{(i)}}\frac{\bar{b}_i}{\bar{R}_i}\left\{-n\frac{\pi}{\varphi_0}\bar{V}_{mn}^{(i)} + \bar{W}_{mn}^{(i)}\right\}\right] \tag{A1}$$

$$\frac{\mathrm{d}\bar{V}_{mn}^{(i)}}{\mathrm{d}\xi} = \left[\frac{h_2^2}{R_2^2}\frac{\bar{b}_i}{\bar{h}_i}\frac{1}{\bar{B}_{66}^{(i)}}\bar{N}_{x\varphi mn}^{(i)} - \frac{\bar{b}_i}{\bar{R}_i}\frac{n\pi}{\varphi_0}\bar{U}_{mn}^{(i)}\right] \tag{A2}$$

$$\frac{\mathrm{d}\bar{W}_{mn}^{(i)}}{\mathrm{d}\xi} = \left[\frac{h_2^2}{R_2^2}\frac{\bar{b}_i}{\bar{h}_i}\frac{1}{\kappa_x^{(i)2}}\frac{1}{\bar{B}_{55}^{(i)}}\bar{Q}_{xzmn}^{(i)} - \frac{R_2}{h_2}\bar{b}_i\bar{\beta}_{xmn}^{(i)}\right] \tag{A3}$$

$$\frac{\mathrm{d}\bar{\beta}_{xmn}^{(i)}}{\mathrm{d}\xi} = \left[12\frac{h_2^2}{R_2^2}\frac{\bar{b}_i}{\bar{h}_i^3}\frac{1}{\bar{B}_{11}^{(i)}}\bar{M}_{xxmn}^{(i)} + \frac{\bar{B}_{12}^{(i)}}{\bar{B}_{11}^{(i)}}\frac{\bar{b}_i}{\bar{R}_i}\frac{n\pi}{\varphi_0}\bar{\beta}_{\varphi mn}^{(i)}\right] \tag{A4}$$

$$\frac{\mathrm{d}\bar{\beta}_{\varphi mn}^{(i)}}{\mathrm{d}\xi} = \left[12\frac{h_2^2}{R_2^2}\frac{\bar{b}_i}{\bar{h}_i^3}\frac{1}{\bar{B}_{66}^{(i)}}\bar{M}_{x\varphi mn}^{(i)} - \frac{\bar{b}_i}{\bar{R}_i}\frac{n\pi}{\varphi_0}\bar{\beta}_{xmn}^{(i)}\right] \tag{A5}$$

where $i = 1, 2$ for the upper and lower shell, respectively.

The first-order system in dimensionless stress resultants are

$$\begin{aligned}\frac{\mathrm{d}\bar{N}_{xxmn}^{(i)}}{\mathrm{d}\xi} = &-\frac{R_2^4}{h_2^4}\bar{G}_a\frac{\bar{b}_i}{\bar{h}_a}\left[(-1)^i + \frac{1}{2}\frac{h_2}{R_2}\frac{\bar{h}_i}{\bar{R}_i}\right]\bar{U}_{mn}^{(1)}\\ &+\frac{R_2^4}{h_2^4}\bar{G}_a\frac{\bar{b}_i}{\bar{h}_a}\left[(-1)^i + \frac{1}{2}\frac{h_2}{R_2}\frac{\bar{h}_i}{\bar{R}_i}\right]\bar{U}_{mn}^{(2)} - \bar{h}_i\bar{b}_i\bar{\rho}_i\bar{\Omega}_{mn}\bar{U}_{mn}^{(i)}\\ &+\frac{1}{2}\frac{R_2^4}{h_2^4}\frac{\bar{h}_1}{\bar{h}_a}\bar{b}_i\bar{G}_a\left\{\left[(-1)^i + \frac{1}{2}\frac{h_2}{R_2}\frac{\bar{h}_i}{\bar{R}_i}\right]\bar{\beta}_{xmn}^{(1)}\right\}\\ &+\frac{1}{2}\frac{R_2^4}{h_2^4}\frac{\bar{b}_i}{\bar{h}_a}\bar{G}_a\left[(-1)^i + \frac{1}{2}\frac{h_2}{R_2}\frac{\bar{h}_i}{\bar{R}_i}\right]\bar{\beta}_{xmn}^{(2)}\end{aligned}$$

$$+\frac{\boldsymbol{R}_2^4}{\boldsymbol{h}_2^4}\bar{\boldsymbol{b}}_i\bar{\boldsymbol{G}}_a\left[(-1)^i+\frac{1}{2}\frac{\boldsymbol{h}_2}{\boldsymbol{R}_2}\frac{\bar{\boldsymbol{h}}_i}{\bar{\boldsymbol{R}}_i}\right]\Delta\bar{\beta}_{xmn}^{(i)}-\frac{\boldsymbol{R}_2}{\boldsymbol{h}_2}\frac{1}{\kappa_x^{(i)^2}}\frac{\bar{\boldsymbol{b}}_i}{\bar{\boldsymbol{h}}_i}\frac{\bar{\boldsymbol{G}}_a}{\bar{\boldsymbol{B}}_{55}^{(i)}}$$
$$\times\left[(-1)^i+\frac{1}{2}\frac{\boldsymbol{h}_2}{\boldsymbol{R}_2}\frac{\bar{\boldsymbol{h}}_i}{\bar{\boldsymbol{R}}_i}\right]\Delta\bar{\boldsymbol{Q}}_{xzmn}^{(i)}+\frac{\bar{\boldsymbol{b}}_i}{\bar{\boldsymbol{R}}_i}\frac{\boldsymbol{n}\pi}{\varphi_0}\bar{\boldsymbol{N}}_{x\varphi mn}^{(i)} \tag{A6}$$

$$\frac{\mathrm{d}\bar{\boldsymbol{N}}_{x\varphi mn}^{(i)}}{\mathrm{d}\xi}=-\frac{\boldsymbol{R}_2^4}{\boldsymbol{h}_2^4}\frac{\bar{\boldsymbol{b}}_i}{\bar{\boldsymbol{h}}_a}\bar{\boldsymbol{G}}_a\left[(-1)^i+\frac{1}{2}\frac{\boldsymbol{h}_2}{\boldsymbol{R}_2}\frac{\bar{\boldsymbol{h}}_i}{\bar{\boldsymbol{R}}_i}\right]\bar{\boldsymbol{V}}_{mn}^{(1)}$$
$$+\frac{\boldsymbol{R}_2^4}{\boldsymbol{h}_2^4}\frac{\bar{\boldsymbol{b}}_i}{\bar{\boldsymbol{h}}_a}\bar{\boldsymbol{G}}_a\left[(-1)^i+\frac{1}{2}\frac{\boldsymbol{h}_2}{\boldsymbol{R}_2}\frac{\bar{\boldsymbol{h}}_i}{\bar{\boldsymbol{R}}_i}\right]\bar{\boldsymbol{V}}_{mn}^{(2)}+\frac{1}{2}\frac{\boldsymbol{R}_2^3}{\boldsymbol{h}_2^3}\frac{\bar{\boldsymbol{b}}_i}{\bar{\boldsymbol{R}}_i}\bar{\boldsymbol{G}}_a$$
$$\times\frac{1}{\left[1+(-1)^i\frac{1}{2}(\boldsymbol{h}_2/\boldsymbol{R}_2)(\bar{\boldsymbol{h}}_i/\bar{\boldsymbol{R}}_i)\right]}\left[(-1)^i\frac{1}{2}\frac{\boldsymbol{h}_2}{\boldsymbol{R}_2}\frac{\bar{\boldsymbol{h}}_i}{\bar{\boldsymbol{R}}_i}\right]\Delta\bar{\boldsymbol{V}}_{mn}^{(i)}$$
$$+\frac{\boldsymbol{R}_2^2}{\boldsymbol{h}_2^2}\frac{\bar{\boldsymbol{h}}_i}{\bar{\boldsymbol{R}}_i^2}\bar{\boldsymbol{b}}_i\left(\frac{\boldsymbol{n}\pi}{\varphi_0}\right)^2\left\{-\frac{\bar{\boldsymbol{B}}_{12}^{(i)}}{\bar{\boldsymbol{B}}_{11}^{(i)}}\bar{\boldsymbol{B}}_{12}^{(i)}+\bar{\boldsymbol{B}}_{22}^{(i)}\right\}\bar{\boldsymbol{V}}_{mn}^{(i)}-\bar{\rho}_i\bar{\boldsymbol{h}}_i\bar{\boldsymbol{b}}_i\bar{\Omega}_{mn}\bar{\boldsymbol{V}}_{mn}^{(i)}$$
$$+\frac{\boldsymbol{R}_2^2}{\boldsymbol{h}_2^2}\frac{\bar{\boldsymbol{h}}_i}{\bar{\boldsymbol{R}}_i^2}\bar{\boldsymbol{b}}_i\left(\frac{\boldsymbol{n}\pi}{\varphi_0}\right)\left[-\frac{\bar{\boldsymbol{B}}_{12}^{(i)}}{\bar{\boldsymbol{B}}_{11}^{(i)}}\bar{\boldsymbol{B}}_{12}^{(i)}-\bar{\boldsymbol{B}}_{22}^{(i)}\right]\bar{W}_{mn}^{(i)}-\frac{\boldsymbol{R}_2^3}{\boldsymbol{h}_2^3}\frac{\bar{\boldsymbol{b}}_i}{\bar{\boldsymbol{R}}_i}\bar{\boldsymbol{G}}_a$$
$$\times\frac{1}{\left[1+(-1)^i\frac{1}{2}(\boldsymbol{h}_2/\boldsymbol{R}_2)(\bar{\boldsymbol{h}}_i/\bar{\boldsymbol{R}}_i)\right]}\left(\frac{\boldsymbol{n}\pi}{\varphi_0}\right)\left[(-1)^i+\frac{1}{2}\frac{\boldsymbol{h}_2}{\boldsymbol{R}_2}\frac{\bar{\boldsymbol{h}}_i}{\bar{\boldsymbol{R}}_i}\right]$$
$$\times\Delta\bar{\boldsymbol{W}}_{mn}^{(i)}+\frac{1}{2}\frac{\boldsymbol{R}_2^4}{\boldsymbol{h}_2^4}\bar{\boldsymbol{b}}_i\frac{\bar{\boldsymbol{h}}_1}{\bar{\boldsymbol{h}}_a}\bar{\boldsymbol{G}}_a\left[(-1)^i+\frac{1}{2}\frac{\boldsymbol{h}_2}{\boldsymbol{R}_2}\frac{\bar{\boldsymbol{h}}_i}{\bar{\boldsymbol{R}}_i}\right]\bar{\beta}_{\varphi mn}^{(1)}$$
$$+\frac{1}{2}\frac{\boldsymbol{R}_2^4}{\boldsymbol{h}_2^4}\frac{\bar{\boldsymbol{b}}_i}{\bar{\boldsymbol{h}}_a}\bar{\boldsymbol{G}}_a\left[(-1)^i+\frac{1}{2}\frac{\boldsymbol{h}_2}{\boldsymbol{R}_2}\frac{\bar{\boldsymbol{h}}_i}{\bar{\boldsymbol{R}}_i}\right]\bar{\beta}_{\varphi mn}^{(2)}+\frac{1}{2}\frac{\boldsymbol{R}_2^3}{\boldsymbol{h}_2^3}\frac{\bar{\boldsymbol{b}}_i}{\bar{\boldsymbol{R}}_i}\bar{\boldsymbol{G}}_a$$
$$\times\frac{(-1)^i\bar{\boldsymbol{h}}_i}{\left[1+(-1)^i\frac{1}{2}(\boldsymbol{h}_2/\boldsymbol{R}_2)(\bar{\boldsymbol{h}}_i/\bar{\boldsymbol{R}}_i)\right]}\left[(-1)^i+\frac{1}{2}\frac{\boldsymbol{h}_2}{\boldsymbol{R}_2}\frac{\bar{\boldsymbol{h}}_i}{\bar{\boldsymbol{R}}_i}\right]\Delta\bar{\beta}_{\varphi mn}^{(i)}$$
$$-\left(\frac{\boldsymbol{n}\pi}{\varphi_0}\right)\frac{\bar{\boldsymbol{b}}_i}{\bar{\boldsymbol{R}}_i}\frac{\bar{\boldsymbol{B}}_{12}^{(i)}}{\bar{\boldsymbol{B}}_{11}^{(i)}}\bar{\boldsymbol{N}}_{xxmn}^{(i)} \tag{A7}$$

$$\frac{\mathrm{d}\bar{\boldsymbol{Q}}_{xzmn}^{(i)}}{\mathrm{d}\xi}=\frac{\boldsymbol{R}_2^2}{\boldsymbol{h}_2^2}\frac{\bar{\boldsymbol{b}}_i}{\bar{\boldsymbol{R}}_i^2}\bar{\boldsymbol{h}}_i\left(\frac{\boldsymbol{n}\pi}{\varphi_0}\right)\left\{\bar{\boldsymbol{B}}_{12}^{(i)}\frac{\bar{\boldsymbol{B}}_{12}^{(i)}}{\bar{\boldsymbol{B}}_{11}^{(i)}}-\bar{\boldsymbol{B}}_{22}^{(i)}-\kappa_\varphi^{(i)^2}\bar{\boldsymbol{B}}_{44}^{(i)}\right\}\bar{\boldsymbol{V}}_{mn}^{(1)}$$
$$-\frac{\boldsymbol{R}_2^4}{\boldsymbol{h}_2^4}\bar{\boldsymbol{E}}_a\frac{\bar{\boldsymbol{b}}_i}{\bar{\boldsymbol{h}}_a}\left\{\left[(-1)^i+\frac{1}{2}\frac{\boldsymbol{h}_2}{\boldsymbol{R}_2}\frac{\bar{\boldsymbol{h}}_i}{\bar{\boldsymbol{R}}_i}\right]\bar{\boldsymbol{W}}_{mn}^{(1)}\right\}$$
$$+\frac{\boldsymbol{R}_2^4}{\boldsymbol{h}_2^4}\bar{\boldsymbol{E}}_a\frac{\bar{\boldsymbol{b}}_i}{\bar{\boldsymbol{h}}_a}\left\{\left[(-1)^i+\frac{1}{2}\frac{\boldsymbol{h}_2}{\boldsymbol{R}_2}\frac{\bar{\boldsymbol{h}}_i}{\bar{\boldsymbol{R}}_i}\right]\bar{\boldsymbol{W}}_{mn}^{(2)}\right\}$$
$$+\frac{\boldsymbol{R}_2^2}{\boldsymbol{h}_2^2}\frac{\bar{\boldsymbol{b}}_i}{\bar{\boldsymbol{R}}_i^2}\bar{\boldsymbol{h}}_i\left\{-\bar{\boldsymbol{B}}_{12}^{(i)}\frac{\bar{\boldsymbol{B}}_{12}^{(i)}}{\bar{\boldsymbol{B}}_{11}^{(i)}}+\bar{\boldsymbol{B}}_{22}^{(i)}+\kappa_\varphi^{(i)^2}\bar{\boldsymbol{B}}_{44}^{(i)}\left(\frac{\boldsymbol{n}\pi}{\varphi_0}\right)^2\right\}\bar{\boldsymbol{W}}_{mn}^{(i)}$$
$$-\bar{\rho}_i\bar{\boldsymbol{h}}_i\bar{\boldsymbol{b}}_i\bar{\Omega}_{mn}\bar{\boldsymbol{W}}_{mn}^{(i)}+\left(\frac{\boldsymbol{R}_2}{\boldsymbol{h}_2}\right)^3\frac{\bar{\boldsymbol{b}}_i}{\bar{\boldsymbol{R}}_i}\bar{\boldsymbol{h}}_i\bar{\boldsymbol{B}}_{44}^{(i)}\kappa_\varphi^{(i)^2}\left(\frac{\boldsymbol{n}\pi}{\varphi_0}\right)\bar{\beta}_{\varphi mn}^{(i)}$$
$$+\frac{\bar{\boldsymbol{b}}_i}{\bar{\boldsymbol{R}}_i}\frac{\bar{\boldsymbol{B}}_{12}^{(i)}}{\bar{\boldsymbol{B}}_{11}^{(i)}}\bar{\boldsymbol{N}}_{xxmn}^{(i)} \tag{A8}$$

$$\frac{\mathrm{d}\bar{\boldsymbol{M}}_{xxmn}^{(i)}}{\mathrm{d}\xi}=\frac{1}{2}\frac{\boldsymbol{R}_2^4}{\boldsymbol{h}_2^4}\frac{\bar{\boldsymbol{h}}_i}{\bar{\boldsymbol{h}}_a}\bar{\boldsymbol{b}}_i\bar{\boldsymbol{G}}_a\left[1+(-1)^i+\frac{1}{2}\frac{\boldsymbol{h}_2}{\boldsymbol{R}_2}\frac{\bar{\boldsymbol{h}}_i}{\bar{\boldsymbol{R}}_i}\right]\bar{\boldsymbol{U}}_{mn}^{(1)}$$
$$+\frac{1}{2}\frac{\boldsymbol{R}_2^4}{\boldsymbol{h}_2^4}\bar{\boldsymbol{b}}_i\frac{\bar{\boldsymbol{h}}_i}{\bar{\boldsymbol{h}}_a}\bar{\boldsymbol{G}}_a\left[1+(-1)^i\frac{1}{2}\frac{\boldsymbol{h}_2}{\boldsymbol{R}_2}\frac{\bar{\boldsymbol{h}}_i}{\bar{\boldsymbol{R}}_i}\right]\bar{\boldsymbol{U}}_{mn}^{(2)}$$
$$+\frac{1}{4}\frac{\boldsymbol{R}_2^4}{\boldsymbol{h}_2^4}\bar{\boldsymbol{b}}_i\bar{\boldsymbol{h}}_1\frac{\bar{\boldsymbol{h}}_i}{\bar{\boldsymbol{h}}_a}\bar{\boldsymbol{G}}_a\left[1+(-1)^i\frac{1}{2}\frac{\boldsymbol{h}_2}{\boldsymbol{R}_2}\frac{\bar{\boldsymbol{h}}_i}{\bar{\boldsymbol{R}}_i}\right]\bar{\beta}_{xmn}^{(1)}$$
$$+\frac{1}{4}\frac{\boldsymbol{R}_2^4}{\boldsymbol{h}_2^4}\bar{\boldsymbol{b}}_i\frac{\bar{\boldsymbol{h}}_i}{\bar{\boldsymbol{h}}_a}\bar{\boldsymbol{G}}_a\left[1+(-1)^i\frac{1}{2}\frac{\boldsymbol{h}_2}{\boldsymbol{R}_2}\frac{\bar{\boldsymbol{h}}_i}{\bar{\boldsymbol{R}}_i}\right]\bar{\beta}_{xmn}^{(2)}$$
$$+\frac{1}{2}\frac{\boldsymbol{R}_2^4}{\boldsymbol{h}_2^4}\bar{\boldsymbol{b}}_i\bar{\boldsymbol{h}}_i\bar{\boldsymbol{G}}_a\left[1+(-1)^i\frac{1}{2}\frac{\boldsymbol{h}_2}{\boldsymbol{R}_2}\frac{\bar{\boldsymbol{h}}_i}{\bar{\boldsymbol{R}}_i}\right]\Delta\bar{\beta}_{xmn}^{(i)}$$
$$-\frac{1}{12}\bar{\rho}_i\bar{\boldsymbol{h}}_i^3\bar{\boldsymbol{b}}_i\bar{\Omega}_{mn}\bar{\beta}_{xmn}^{(i)}+\frac{\bar{\boldsymbol{b}}_i}{\bar{\boldsymbol{R}}_i}\left(\frac{\boldsymbol{n}\pi}{\varphi_0}\right)\bar{\boldsymbol{M}}_{x\varphi mn}^{(i)}+\frac{\boldsymbol{R}_2}{\boldsymbol{h}_2}\bar{\boldsymbol{b}}_i\bar{\boldsymbol{Q}}_{xzmn}^{(i)}$$
$$-\frac{1}{2}\frac{\boldsymbol{R}_2}{\boldsymbol{h}_2}\frac{1}{\kappa_x^{(i)^2}}\bar{\boldsymbol{b}}_i\frac{\bar{\boldsymbol{G}}_a}{\bar{\boldsymbol{B}}_{55}^{(i)}}\left\{1+(-1)^i\frac{1}{2}\frac{\boldsymbol{h}_2}{\boldsymbol{R}_2}\frac{\bar{\boldsymbol{h}}_i}{\bar{\boldsymbol{R}}_i}\right\}\Delta\bar{\boldsymbol{Q}}_{xzmn}^{(i)} \tag{A9}$$

$$\frac{\mathrm{d}\bar{\boldsymbol{M}}_{x\varphi mn}^{(i)}}{\mathrm{d}\xi}=-\frac{1}{2}\frac{\boldsymbol{R}_2^4}{\boldsymbol{h}_2^4}\bar{\boldsymbol{b}}_i\frac{\bar{\boldsymbol{h}}_i}{\bar{\boldsymbol{h}}_a}\bar{\boldsymbol{G}}_a\left[1+(-1)^i\frac{1}{2}\frac{\boldsymbol{h}_2}{\boldsymbol{R}_2}\frac{\bar{\boldsymbol{h}}_i}{\bar{\boldsymbol{R}}_i}\right]\bar{\boldsymbol{V}}_{mn}^{(1)}$$
$$+\frac{1}{2}\frac{\boldsymbol{R}_2^4}{\boldsymbol{h}_2^4}\bar{\boldsymbol{b}}_i\frac{\bar{\boldsymbol{h}}_i}{\bar{\boldsymbol{h}}_a}\bar{\boldsymbol{G}}_a\left[1+(-1)^i\frac{1}{2}\frac{\boldsymbol{h}_2}{\boldsymbol{R}_2}\frac{\bar{\boldsymbol{h}}_i}{\bar{\boldsymbol{R}}_i}\right]\bar{\boldsymbol{V}}_{mn}^{(2)}$$
$$-\left(\frac{\boldsymbol{R}_2}{\boldsymbol{h}_2}\right)^3\kappa_\varphi^{(i)^2}\bar{\boldsymbol{h}}_i\frac{\bar{\boldsymbol{b}}_i}{\bar{\boldsymbol{R}}_i}\bar{\boldsymbol{B}}_{44}^{(i)}\bar{\boldsymbol{V}}_{mn}^{(i)}+\frac{1}{4}\frac{\boldsymbol{R}_2^3}{\boldsymbol{h}_2^3}\frac{\bar{\boldsymbol{b}}_i}{\bar{\boldsymbol{R}}_i}\bar{\boldsymbol{G}}_a$$
$$\times\frac{\bar{\boldsymbol{h}}_i}{\left[1+(-1)^i\frac{1}{2}(\boldsymbol{h}_2/\boldsymbol{R}_2)(\bar{\boldsymbol{h}}_i/\bar{\boldsymbol{R}}_i)\right]}\left[1+(-1)^i\frac{1}{2}\frac{\boldsymbol{h}_2}{\boldsymbol{R}_2}\frac{\bar{\boldsymbol{h}}_i}{\bar{\boldsymbol{R}}_i}\right]\Delta\bar{\boldsymbol{V}}_{mn}^{(i)}$$
$$+\left(\frac{\boldsymbol{R}_2}{\boldsymbol{h}_2}\right)^3\kappa_\varphi^{(i)^2}\left(\frac{\boldsymbol{n}\pi}{\varphi_0}\right)\bar{\boldsymbol{h}}_i\frac{\bar{\boldsymbol{b}}_i}{\bar{\boldsymbol{R}}_i}\bar{\boldsymbol{B}}_{44}^{(i)}\bar{\boldsymbol{W}}_{mn}^{(i)}-\frac{1}{2}\frac{\boldsymbol{R}_2^3}{\boldsymbol{h}_2^3}\left(\frac{\boldsymbol{n}\pi}{\varphi_0}\right)\frac{\bar{\boldsymbol{b}}_i}{\bar{\boldsymbol{R}}_i}$$
$$\times\frac{\bar{\boldsymbol{h}}_i}{\left[1+(-1)^i\frac{1}{2}(\boldsymbol{h}_2/\boldsymbol{R}_2)(\bar{\boldsymbol{h}}_i/\bar{\boldsymbol{R}}_i)\right]}\bar{\boldsymbol{G}}_a\left\{1+(-1)^i\frac{1}{2}\frac{\boldsymbol{h}_2}{\boldsymbol{R}_2}\frac{\bar{\boldsymbol{h}}_i}{\bar{\boldsymbol{R}}_i}\right\}$$
$$\times\Delta\bar{\boldsymbol{W}}_{mn}^{(i)}+\frac{1}{4}\frac{\boldsymbol{R}_2^4}{\boldsymbol{h}_2^4}\bar{\boldsymbol{G}}_a\bar{\boldsymbol{b}}_i\bar{\boldsymbol{h}}_1\frac{\bar{\boldsymbol{h}}_i}{\bar{\boldsymbol{h}}_a}\left[1+(-1)^i\frac{1}{2}\frac{\boldsymbol{h}_2}{\boldsymbol{R}_2}\frac{\bar{\boldsymbol{h}}_i}{\bar{\boldsymbol{R}}_i}\right]\bar{\beta}_{\varphi mn}^{(1)}$$
$$+\frac{1}{4}\frac{\boldsymbol{R}_2^4}{\boldsymbol{h}_2^4}\bar{\boldsymbol{b}}_i\frac{\bar{\boldsymbol{h}}_i}{\bar{\boldsymbol{h}}_a}\bar{\boldsymbol{G}}_a\left[1+(-1)^i\frac{1}{2}\frac{\boldsymbol{h}_2}{\boldsymbol{R}_2}\frac{\bar{\boldsymbol{h}}_i}{\bar{\boldsymbol{R}}_i}\right]\bar{\beta}_{\varphi mn}^{(2)}+\left(\frac{\boldsymbol{R}_2}{\boldsymbol{h}_2}\right)^2\bar{\boldsymbol{h}}_i^3\bar{\boldsymbol{b}}_i$$
$$\times\left[\frac{1}{12}\frac{1}{\bar{\boldsymbol{R}}_i^2}\left(\frac{\boldsymbol{n}\pi}{\varphi_0}\right)^2\left\{-\bar{\boldsymbol{B}}_{12}^{(i)}\frac{\bar{\boldsymbol{B}}_{12}^{(i)}}{\bar{\boldsymbol{B}}_{11}^{(i)}}-\bar{\boldsymbol{B}}_{22}^{(i)}\right\}+\kappa_\varphi^{(i)^2}\left(\frac{\boldsymbol{R}_2}{\boldsymbol{h}_2}\right)^2\frac{1}{\bar{\boldsymbol{h}}_i^2}\bar{\boldsymbol{B}}_{44}^{(i)}\right]$$
$$\times\bar{\beta}_{\varphi mn}^{(i)}+\frac{1}{4}\frac{\boldsymbol{R}_2^3}{\boldsymbol{h}_2^3}\frac{\bar{\boldsymbol{b}}_i}{\bar{\boldsymbol{R}}_i}(-1)^i\frac{\bar{\boldsymbol{h}}_i^2}{\left[1+(-1)^i\frac{1}{2}(\boldsymbol{h}_2/\boldsymbol{R}_2)(\bar{\boldsymbol{h}}_i/\bar{\boldsymbol{R}}_i)\right]}\bar{\boldsymbol{G}}_a$$
$$\times\left[1+(-1)^i\frac{1}{2}\frac{\boldsymbol{h}_2}{\boldsymbol{R}_2}\frac{\bar{\boldsymbol{h}}_i}{\bar{\boldsymbol{R}}_i}\right]\Delta\bar{\beta}_{\varphi mn}^{(i)}-\frac{1}{12}\bar{\boldsymbol{h}}_i^3\bar{\rho}_i\bar{\boldsymbol{b}}_i\bar{\Omega}_{mn}\bar{\beta}_{\varphi mn}^{(i)}$$
$$-\frac{\bar{\boldsymbol{B}}_{12}^{(i)}}{\bar{\boldsymbol{B}}_{11}^{(i)}}\frac{\bar{\boldsymbol{b}}_i}{\bar{\boldsymbol{R}}_i}\left(\frac{\boldsymbol{n}\pi}{\varphi_0}\right)\bar{\boldsymbol{M}}_{xxmn}^{(i)} \tag{A10}$$

where $i=1,2$ for the upper and lower shell, respectively, and κ_x and κ_φ are the shear correction factors in the $\boldsymbol{x}$ the and φ directions, respectively.[24]

Appendix B: Discretization

The discretized dimensionless fundamental dependent variables and discretized modified transfer matrix $[\dot{\mathcal{U}}]$ (for the part I region) are

$$\left\{\left[\bar{\boldsymbol{U}}_1^{(1)}\quad\bar{\boldsymbol{U}}_2^{(1)}\quad\cdots\quad\bar{\boldsymbol{U}}_k^{(1)}\right],\left[\bar{\boldsymbol{V}}_1^{(1)}\quad\bar{\boldsymbol{V}}_2^{(1)}\quad\cdots\quad\bar{\boldsymbol{V}}_k^{(1)}\right],\ldots,\right.$$
$$\left[\bar{\boldsymbol{Q}}_{xz1}^{(1)}\quad\bar{\boldsymbol{Q}}_{xz2}^{(1)}\quad\cdots\quad\bar{\boldsymbol{Q}}_{xzk}^{(1)}\right];\left[\bar{\boldsymbol{U}}_1^{(2)}\quad\bar{\boldsymbol{U}}_2^{(2)}\quad\cdots\quad\bar{\boldsymbol{U}}_k^{(2)}\right]$$
$$\left.\left[\bar{\boldsymbol{V}}_1^{(2)}\quad\bar{\boldsymbol{V}}_2^{(2)}\quad\cdots\quad\bar{\boldsymbol{V}}_k^{(2)}\right],\ldots,\left[\bar{\boldsymbol{Q}}_{xz1}^{(2)}\quad\bar{\boldsymbol{Q}}_{xz2}^{(2)}\quad\cdots\quad\bar{\boldsymbol{Q}}_{xzk}^{(2)}\right]\right\}^T$$
$$=[\dot{\mathcal{U}}]\left\{\left[\bar{\boldsymbol{U}}_1^{(1)}\quad\bar{\boldsymbol{U}}_1^{(1)}\quad\cdots\quad\bar{\boldsymbol{U}}_1^{(1)}\right],\left[\bar{\boldsymbol{V}}_1^{(1)}\quad\bar{\boldsymbol{V}}_1^{(1)}\quad\cdots\quad\bar{\boldsymbol{V}}_1^{(1)}\right],\right.$$
$$\ldots,\left[\bar{\boldsymbol{Q}}_{xz1}^{(1)}\quad\bar{\boldsymbol{Q}}_{xz1}^{(1)}\quad\cdots\quad\bar{\boldsymbol{Q}}_{xz1}^{(1)}\right],\left[\bar{\boldsymbol{U}}_1^{(2)}\quad\bar{\boldsymbol{U}}_1^{(2)}\quad\cdots\quad\bar{\boldsymbol{U}}_1^{(2)}\right],$$
$$\left.\left[\bar{\boldsymbol{V}}_1^{(2)}\quad\bar{\boldsymbol{V}}_1^{(2)}\quad\cdots\quad\bar{\boldsymbol{V}}_1^{(2)}\right],\ldots,\left[\bar{\boldsymbol{Q}}_{xz1}^{(2)}\quad\bar{\boldsymbol{Q}}_{xz1}^{(2)}\quad\cdots\quad\bar{\boldsymbol{Q}}_{xz1}^{(2)}\right]\right\}^T \tag{B1}$$

The final form of the modified transfer matrix $[\tilde{\mathcal{U}}]_{01}$ in detail (for the part I region) is

$$\begin{Bmatrix} \bar{U}^{(1)}_{\xi_I=1} \\ \bar{V}^{(1)}_{\xi_I=1} \\ \cdot \\ \cdot \\ \bar{Q}^{(1)}_{xz_{\xi_I=1}} \\ --- \\ \bar{U}^{(2)}_{\xi_I=1} \\ \bar{V}^{(2)}_{\xi_I=1} \\ \cdot \\ \cdot \\ \bar{Q}^{(2)}_{xz_{\xi_I=1}} \end{Bmatrix} = [\tilde{\mathcal{U}}]_{01} \begin{Bmatrix} \bar{U}^{(1)}_{\xi_I=0} \\ \bar{V}^{(1)}_{\xi_I=0} \\ \cdot \\ \cdot \\ \bar{Q}^{(1)}_{xz_{\xi_I=0}} \\ --- \\ \bar{U}^{(2)}_{\xi_I=0} \\ \bar{V}^{(2)}_{\xi_I=0} \\ \cdot \\ \cdot \\ \bar{Q}^{(2)}_{xz_{\xi_I=0}} \end{Bmatrix}$$

$$[\tilde{\mathcal{U}}]_{01} = \begin{bmatrix} \sum_{i=1}^{k} \dot{\mathcal{U}}_{k,i} & \sum_{i=k+1}^{2k} \dot{\mathcal{U}}_{k,i} & \cdot & \cdot & \sum_{i=19k+1}^{20k} \dot{\mathcal{U}}_{k,i} \\ \sum_{i=1}^{k} \dot{\mathcal{U}}_{2k,i} & \cdot & \cdot & \cdot & \cdot \\ \cdot & \cdot & \cdot & \cdot & \cdot \\ \cdot & \cdot & \cdot & \cdot & \sum_{i=19k+1}^{20k} \dot{\mathcal{U}}_{19k,i} \\ \sum_{i=1}^{k} \dot{\mathcal{U}}_{20k,i} & \cdot & \cdot & \sum_{i=18k+1}^{19k} \dot{\mathcal{U}}_{20k,i} & \sum_{i=19k+1}^{20k} \dot{\mathcal{U}}_{20k,i} \end{bmatrix} \tag{B2}$$

where k is the number of discretizing points along the ξ_I direction and superscripts 1 and 2 indicate upper and lower shell layers, respectively.

Appendix C: Adhesive Stresses

The adhesive-layer transverse normal and shear stresses (at upper, $i=1$, and lower, $i=2$, shell–adhesive-layer interfaces) are

$$\tau^{(i)}_{zx} = \boldsymbol{G}_a \gamma^{(i)}_{zx} = (\boldsymbol{G}_a/\boldsymbol{h}_a)\left\{\left[\boldsymbol{u}^{(1)} - (\boldsymbol{h}_1/2)\beta^{(1)}_x - \boldsymbol{u}^{(2)} - (\boldsymbol{h}_2/2)\beta^{(2)}_x\right]\right\} + \Delta_1$$

$$\tau^{(i)}_{z\varphi} = \boldsymbol{G}_a \gamma^{(i)}_{z\varphi} = (\boldsymbol{G}_a/\boldsymbol{h}_a)\left\{\left[\boldsymbol{v}^{(1)} - (\boldsymbol{h}_1/2)\beta^{(1)}_\varphi - \boldsymbol{v}^{(2)} - (\boldsymbol{h}_2/2)\beta^{(2)}_\varphi\right]\right\} - \Delta_2, \qquad (i=1,2)$$

$$\sigma^{(i)}_z = \boldsymbol{E}_a \varepsilon^{(i)}_z = (\boldsymbol{E}_a/\boldsymbol{h}_a)\left(\boldsymbol{w}^{(1)} - \boldsymbol{w}^{(2)}\right) \tag{C1}$$

where $\boldsymbol{E}_a$ and $\boldsymbol{G}_a$ are the adhesive elastic constants and Δ are derived from the curvature of shells. (The adhesive-layer stresses act as surface loads on shells in the part I region in the dynamic equations of Appendix A.)

References

[1]Hoskins, B. C., and Baker, A. A., *Composite Materials for Aircraft Structures*, AIAA Educational Series, AIAA, New York, 1986.

[2]Marshall, I. H., and Demuts, E. (eds.), *Supportability of Composite Airframes and Structures*, Elsevier Applied Science, New York, 1988.

[3]Smith, P. J., Ilcewicz, L. B., and Olson, Y. T., "Advanced Technology Composite Fuselage," *Proceedings of the 5th NASA/DOD/ARPA Advanced Composites Technology Conference*, NASA Langley Research Center, 1995, pp. 1–31; also NASA CP-3294, 1995.

[4]Adams, R. D., and Peppiatt, N. A., "Stress Analysis of Adhesively Bonded Tubular Lap Joints," *Journal of Adhesion*, Vol. 9, No. 1, 1977, pp. 1–18.

[5]Lubkin, J. L., and Reissner, E., "Stress Distribution and Design Data for Adhesive Joints Between Circular Tubes," *Journal of Applied Mechanics*, Vol. 78, 1956, pp. 1213–1221.

[6]Rao, M. D., and Zhou, H., "Vibration and Damping of a Bonded Tubular lap Joint," *Journal of Sound and Vibration*, Vol. 178, No. 5, 1994, pp. 577–590.

[7]Yuceoglu, U., and Updike, D. P., "Stress Concentrations in Bonded Multi-Layer Cylindrical Shells," American Society of Civil Engineers, Engineering Mechanics Div. Preprint 80-656, 1980; also ASCE Engineering Mechanics Division Conf., Hollywood, FL, 1980.

[8]Yuceoglu, U., and Updike, D. P., "On the Analysis of Adhesive Joints in Fiber-Reinforced Composite Plates and Shells," *Advances in Aerospace Structures and Materials*, edited by R. M. Laurenson and U. Yuceoglu, American Society of Mechanical Engineers, New York, 1982, pp. 19–24.

[9]Yuceoglu, U., and Updike, D. P., "Tubular Shell Lap Joints in Composite Cylindrical Shells Under Extension and Bending," *Proceedings of the 4th International Conference on Composite Materials*, Vol. 1, Progress in Science and Engineering of Composites, Japanese Society of Composites, Tokyo, 1982, pp. 297–304.

[10]Yuceoglu, U., and Özerciyes, V., "Natural Frequencies and Mode Shapes of Composite Plates or Panels with a Central Stiffening Plate Strip," *Symposium on Vibroacoustic Methods in Processing and Characterization of Advanced Materials and Structures*, NCA-Vol. 24, American Society of Mechanical Engineers, 1997, pp. 185–196.

[11]Yuceoglu, U., and Özerciyes, V., "Sudden Drop Phenomena in Natural Frequencies of Partially Stiffened, Stepped-Thickness, Composite Plates or Panels," *Proceedings of the 40th AIAA/ASME/ASCE/AHS/ASC Structures, Structural Dynamics, and Materials Conference*, AIAA, Reston, VA, 1999, pp. 2336–2347.

[12]Yuceoglu, U., and Özerciyes, V., "Natural Frequencies and Mode Shapes of Stepped-Thickness and/or Stiffened Plates and Panels," AIAA Paper 2000-1348, 2000.

[13]Yuceoglu, U., and Özerciyes, V., "Sudden Drop Phenomena in Natural Frequencies of Composite Plates or Panels with a Central Stiffening Plate Strip," *International Journal of Computers and Structures*, Vol. 76, No. 1–3 (Special Issue), 2000, pp. 247–262.

[14]Yuceoglu, U., and Özerciyes, V., "Free Vibrations of Composite, Shallow Circular Cylindrical Shell Panels with a Bonded Central Stiffening Shell Strip," *Symposium in Honor of Prof. G. J. Smitses*, 2001 ASME International Mechanical Engineering Congress and Exposition, American Society of Mechanical Engineers, 2001.

[15]Yuceoglu, U., and Özerciyes, V., "Free Flexural Vibrations of Orthotropic Composite Base Plates or Panels with a Bonded Noncentral (or Eccentric) Stiffening Plate Strip," *Journal of Vibration and Acoustics*, Vol. 125, No. 2, 2003, pp. 228–243.

[16]Leissa, A. W., *Vibration of Shells*, NASA SP-228, 1973.

[17]Markus, S., *The Mechanics of Vibrations of Cylindrical Shells*, Studies in Applied Mechanics, Elsevier Science, New York, 1988.

[18]Soedel, W., "On the Vibrations of Shells with Timoshenko–Mindlin Type Shear Deflections and Rotatory Inertia," *Journal of Sound and Vibration*, Vol. 83, No. 1, 1982, pp. 67–79.

[19]Soedel, W., *Vibrations of Shells and Plates*, 2nd ed., Marcel Dekker, New York, 1993.

[20]Yamada, G., Irie, T., and Shoji, N., "Vibration Characteristics of a Cylindrically Curved Thick Plate," *Journal of Sound and Vibration*, Vol. 110, No. 2, 1986, pp. 337–346.

[21]Reddy, J. N., and Liu, C. F., "Higher Order Shear Deformation Theory of Laminated Elastic Shells," *International Journal of Engineering Science*, Vol. 23, No. 3, 1985, pp. 319–330.

[22]Noor, A. K., and Burton, W. S., "Assessment of Computational Models for Multi-Layered Composite Shells," *Applied Mechanics Reviews*, Vol. 43, No. 4, 1990, pp. 67–97.

[23]Yuceoglu, U., Toghi, F., and Tekinalp, O., "Free Bending Vibrations of Adhesively Bonded, Orthotropic Plates with a Single Lap Joint," *Journal of Vibration and Acoustics*, Vol. 118, No. 1, 1996, pp. 122–134.

[24]Wittrick, W. H., "Analytical Three-Dimensional Solutions to Some Plate Problems and Some Observations on Mindlin Plate Theory," *International Journal of Solids and Structures*, Vol. 23, No. 2, 1987, pp. 441, 464.

[25]Warburton, G. B., *The Dynamical Behaviour of Structures*, 2nd ed., Pergamon, New York, 1976, pp. 273–277.

A. Palazotto
Associate Editor